ROBUST AND FAST BASS LOCAL VOLATILITY

Hao Qin[†], ◉ **Charlie Che**[†‡]**, Ruozhong Yang**[†]**, and Liming Feng**[†*]

[†]Department of Industrial and Enterprise Systems Engineering, University of Illinois Urbana-Champaign, Illinois, United States
[‡]JPMorgan Chase & Co., New York, United States

ABSTRACT

The Bass Local Volatility Model (Bass-LV), as studied in [Conze and Henry-Labordere, 2021], stands out for its ability to eliminate the need for interpolation between maturities. This offers a significant advantage over traditional LV models. However, its performance highly depends on accurate construction of state price densities and the corresponding marginal distributions and efficient numerical convolutions which are necessary when solving the associated fixed point problems. In this paper, we propose a new approach combining local quadratic estimation and lognormal mixture tails for the construction of state price densities. We investigate computational efficiency of trapezoidal rule based schemes for numerical convolutions and show that they outperform commonly used Gauss-Hermite quadrature. We demonstrate the performance of the proposed method, both in standard option pricing models, as well as through a detailed market case study.

Keywords: Bass Local Volatility, state price density, local quadratic estimation, lognormal mixture tails, numerical integration, trapezoidal rule

1 Introduction

In derivatives pricing, the local volatility (LV) model has been widely adopted, particularly in applications involving the calibration of exotic options[Derman et al., 1996][Coleman et al., 2001][Bouzoubaa and Osseiran, 2010][Kotzé et al., 2015]. Dupire's formulation of LV models provides a deterministic framework where instantaneous volatility is a function of both the asset price and time. Since Dupire's seminal work, this framework has become a key tool and industry standard for capturing the dynamics of underlying asset prices. However, practical application of such models faces challenges due to the lack of observable vanilla prices across all strikes and maturities. One of the main challenges is the need for an arbitrage-free interpolation scheme for volatilities at unobserved maturities. The time interpolation and related extrapolation can introduce instabilities and make the model highly sensitive to variations in market data.

This issue can be effectively addressed by the Bass-LV construction proposed by [Conze and Henry-Labordere, 2021]. The Bass-LV construction, rooted in the Bass martingale, is a solution to the Martingale Benamou-Brenier problem introduced by [Backhoff et al., 2017]. Bass-LV model leverages the martingale property of the asset price process to ensure the absence of calendar arbitrage, thereby circumventing the need for direct time interpolation of volatilities. This construction is particularly advantageous because it aligns with the martingale condition, which is a fundamental requirement for no-arbitrage pricing in financial markets.

The Bass-LV model is particularly well-suited for pricing a wide array of exotic payoffs, such as autocalls, forward-start options, lookback options, and Asian options. Its accuracy and flexibility in addressing the complex and diverse needs of exotic option pricing make Bass-LV a competitive choice in volatility modeling. The model takes inputs of implied marginal distributions and calibrates the spot price process through specific numerical convolution schemes using a fixed-point algorithm, enabling Monte Carlo simulation to derive vanilla option prices and the corresponding implied volatility (IV) smile for the market.

---

[*]Corresponding author. Email: fenglm@illinois.edu

Recent theoretical work by [Acciaio et al., 2023] further substantiates the Bass-LV model, showing linear convergence rate of the numerical scheme in the fixed-point algorithm. [Tschiderer, 2024] extends the Bass-LV construction by replacing the Gaussian transition kernel with an arbitrary reference measure q, thus provides more flexibility in fitting different financial assets. [Loeper, 2023] introduces additional PDE methods for computing the fixed-point iteration, which offers alternative approaches to the calibration process. Moreover, [Backhoff-Veraguas et al., 2023a] and [Backhoff-Veraguas et al., 2023b] give general theoretical results by analyzing the dual formulation of the Bass martingale, and strengthen the model's theoretical foundation.

The concept of leveraging martingales in Bass-LV is indeed a part of Martingale Optimal Transport (MOT) frameworks, which extends the classical Optimal Transport problem [Monge, 1781] by incorporating the martingale property. Beyond the Bass-LV construction, a variety of research has explored alternative MOT frameworks to address different problem settings. For example, [Henry-Labordere, 2019a] gives a new class of stochastic volatility models by combining martingale Schrodinger bridges framework with Sinkhorn algorithm from [De March and Henry-Labordere, 2019]. [Eckstein and Kupper, 2021] gives the feed-forward neural network formulation of MOT problem and enable the neural network solution for problem constructed in high dimensional space with multiple assets. [Henry-Labordere, 2019b] proposes a primal-dual algorithm for solving MOT problems that can leverage the privilege of generative adversarial networks. Other interesting work can been seen in [Hobson and Neuberger, 2012], [Beiglböck et al., 2013], [Dolinsky and Soner, 2014], [Henry-Labordère and Touzi, 2016], [Guo et al., 2017], [Henry-Labordère, 2017], and [Nutz et al., 2023].

Despite the advantages over traditional LV models, Bass-LV model still has some limitations. First, the model relies on a fixed-point algorithm that involves multiple convolutions and integrations implemented with Gauss-Hermite quadrature. Preliminary results suggest that using a small number of quadrature points often compromises accuracy, while increasing the number significantly extends computational time. Second, computing implied state price densities and corresponding marginal distributions of asset prices commonly depends on simple interpolation and extrapolation based on the Breeden-Litzenberger formula. However, these techniques cannot be directly applied due to the arbitrage present in market data. Even after removing arbitrage, tail's accuracy of distribution cannot be guaranteed and may lead to unneglectable instability during calibration process.

These limitations highlight the need for further refinement of the Bass-LV model and its calibration process. Our research aims to address these challenges by proposing more robust numerical schemes and methods that enhance both the stability and accuracy of the Bass-LV model in practical applications.

In this paper, Section 2 provides a review of the mathematical background related to Bass-LV construction. Section 3 leverages a local quadratic regression model with adaptive parameter to generate the non-arbitrage state price density for observable market prices. A mixture of two lognormal distributions approximation is later applied for tails approximation of the density. Section 4 analyzes the theoretical optimality and convergence rate of the Trapezoidal Rule Scheme. It is then compared to Gauss-Hermite quadrature scheme under the settings of Bass-LV model, where finite smoothness is assumed. In section 5, the experiments start with a Black-Scholes example to show the relationship between the iteration tolerance and calibration accuracy for Bass-LV model. Comparison between our proposed method and Breeden-Litzenberger formulation is later done under a case of Heston-like parameterization for random surface Stochastic-Volatility-Inspired model(SSVI). Finally, a market case study is conducted to demonstrate the practical applicability of the proposed method.

2   Background

Bass-LV model stands out as a Markov model that achieves precise calibration to the price distributions $\mu_1, \ldots, \mu_n$ implied from the market prices of vanilla options across a specific range of maturities $0 \leq T_1 < \cdots < T_n$. The core of the Bass-LV model lies in the extension of the Bass martingale construction within the context of the Skorokhod embedding problem. To be specific, given two probability distributions $\mu_i, \mu_{i+1} \in \mathcal{P}(\mathbb{R})$ in convex order, the objective is to construct a martingale $(M_t)_{t \in [T_i, T_{i+1}]}$ with the initial and terminal distributions $M_{T_i} \sim \mu_i$ and $M_{T_{i+1}} \sim \mu_{i+1}$, respectively, where $M_t = f_t(W_t, t)$ for $t \in [T_i, T_{i+1}]$. Here, W_t denotes a predictable right-continuous with left limits (RCLL) process such that $W_t = W_{T_i} + B_t - B_{T_i}$ for all $t \in [T_i, T_{i+1})$, and for all $i = 0, \cdots, n - 1$, with $(B_t)_{0 \leq t \leq T}$ being a standard Brownian motion. Notice, the generalization of Bass-LV from the classical Bass Martingale is indeed not a trivial one. In the classical Bass Martingale case and when the dimension is $\mathbb{R}$, the initial marginal is a Dirac measure, $\mu := \delta_m$ in which m is the mean of ν. It turns out the solution to the martingale optimal transport problem(also known as stretched Brownian Motion) is equivalent to finding the martingale that closely tracks a baseline Brownian motion while respecting the initial and terminal marginals. As such, finding the solution comes down to finding a monotone increasing function $f : \mathbb{R} \mapsto \mathbb{R}$ such that $f(\gamma) = \nu$ where γ is the standard normal distribution on $\mathbb{R}$. The

martingale M_t can be defined as

$$M_t := \mathbb{E}[f(B_1)|\mathscr{F}] = \mathbb{E}[f(B_1)|B_t] = f_t(B_t) \tag{1}$$

This turns out to be trivial to construct. At the terminal, i.e. where f maps from B_1 to ν, f is simply the Frechet Hoeffding solution $f = F_\nu^{-1} \circ F_{B_1} = F_\nu^{-1} \circ \mathcal{N}(\sigma)$ where F and F^{-1} are denoted as the CDF and the inverse CDF of the respective distribution. Given that the lifted space is a Martingale, f must obey the heat equation. In this vein, defining f on all of $t \in [0, 1]$ boils down to solving the heat equation with terminal condition defined by the Frechet Hoeffding solution. From classical PDE theory, this is simply the convolution of the terminal condition with the heat kernel operator.

$$\frac{\partial f}{\partial t} + \frac{1}{2}\frac{\partial^2 f}{\partial \sigma^2}f = 0 \tag{2}$$

$$f(\sigma, 1) = F_\nu^{-1} \circ F_{B_1} \tag{3}$$

$$f(\sigma, t) = \mathcal{K}_{1-t} * f(\sigma, 1) = \mathcal{K}_{1-t} * \left(F_\nu^{-1} \circ F_{B_1}\right) \tag{4}$$

In general, when the initial marginal μ is not trivial, the base process cannot assumed to be reversible. Therefore, finding the optimizer for the Martingale Benamou Brenier problem is equivalent to finding the initial marginal for the base process. Specifically, in the Bass local volatility case, the LV calibration reduces to devising a fixed point algorithm as in [Conze and Henry-Labordere, 2021] to find the initial base distribution of α.
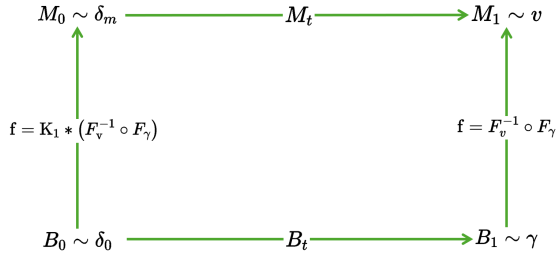

Figure 1: Bass Martingale

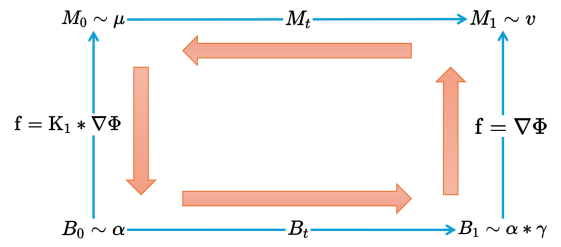

Figure 2: Bass Local Volatility

The function $f_t(x) : [T_i, T_{i+1}] \times \mathbb{R} \to \mathbb{R}$ defines the underlying spot price process S_t between two given maturities.

To calibrate the specific W_t for $t \in [T_i, T_{i+1}]$, one needs to apply a fixed-point algorithm for the cumulative distribution function (CDF) of W_t: $F_{W_{T_i}} = \mathcal{A}F_{W_{T_i}}$, where $\mathcal{A}$ is a nonlinear integration operator $\mathcal{A} : \text{CDF} \to \text{CDF}$ that is given by

$$\mathcal{A}F := F_{\mu_i} \circ \left(K_{T_{i+1}-T_i} \star \left(F_{\mu_{i+1}}^{-1} \circ \left(K_{T_{i+1}-T_i} \star F\right)\right)\right).$$

Here, K is the heat kernel $K_t(x) := \frac{e^{-\frac{x^2}{2t}}}{\sqrt{2\pi t}}$, $\circ$ denotes the composition operator, and $\star$ the convolution.

In numerical practice, we can start the calibration with an initial guess of Gaussian distribution for that specific random process W_t. The spot price process can then be expressed by $f(t, \cdot) = K_{T_{i+1}-t} \star \left(F_{\mu_{i+1}}^{-1} \circ \left(K_{T_{i+1}-T_i} \star F_{W_{T_i}}\right)\right)$, where $F_{W_{T_i}}$ is the converged result for F by applying the appropriate integration techniques in the fixed-point algorithm. The simulation of the call option price follows a common practice, where we utilize the pricing formula Payoff $= \mathbf{E}[(\text{Spot price} - \text{Strikes})^+]$, and then we inversely solve the European call option price formula under the Black-Scholes Model to derive the market smile.

3 Construction of Non-arbitrage State Price Density

In this section, we give details of proposed method for obtaining arbitrage-free state price density from options data, which helps to generate the necessary marginal distribution as inputs for Bass construction by integral. We mainly focus on formulations related to vanilla call options, and results of put options can be obtained similarly.

Consider the European call option pricing formula from the Black-Scholes model:

$$C_t(K, \tau) = S_t \Phi(d_1(K)) - Ke^{-r\tau}\Phi(d_2(K)),$$

where S_t is the stock price at time t, K is the strike price, r is the risk-free interest rate, $\tau = T - t$ is the time-to-maturity, and σ is the constant volatility parameter. The terms d_1 and d_2 are given by:

$$d_1(K) = \frac{\ln\left(S_t/K\right) + \left(r + 0.5\sigma^2\right)\tau}{\sigma\sqrt{\tau}}, \quad d_2(K) = d_1(K) - \sigma\sqrt{\tau},$$

By the Breeden-Litzenberger formulation, we can compute the state price density of specific time to maturity τ as follows

$$q(x) \stackrel{\text{def}}{=} e^{r\tau} \left.\frac{\partial^2 C_t(K,\tau)}{\partial K^2}\right|_{K=x},$$

where we denote $q(x)$ as the price density given a terminal maturity T and current maturity t for a specific strike price x.

Common practice to obtain the state price density is to first apply some smoothing techniques to remove butterfly arbitrage in option prices, and then use the central difference method to approximate the derivatives. However, as we will show later in the numerical experiment section, such methods will be highly sensitive to the number of market observations and will also have significant errors in reproducing the call option prices if the integration of estimated density is significantly deviated from 1.

Instead of directly using the relationship between option price and state price density, we can also treat state price density as a function of IV and its derivatives.

Given that even minor differences in price can lead to substantial differences in IV, especially in the case of near-maturity options, we prefer to use IV rather than price to calculate density for numerical stability. Our assumption is that errors are based on IV, and since the relationship between price and IV is nonlinear, using price could introduce instability into the method.

The deduction based on implied volatility is straightforward from [Benko et al., 2007] where φ is the p.d.f. of a standard normal random variable:

$$
\begin{aligned}
q(x) = & e^{r\tau} S_t \sqrt{\tau} \varphi\left(d_1(x)\right) \left[\frac{1}{x^2 \sigma_t(x,\tau)\tau} + \frac{2d_1(x)}{x\sigma_t(x,\tau)\sqrt{\tau}} \left.\frac{\partial \sigma_t(K,\tau)}{\partial K}\right|_{K=x} \right. \\
& + \frac{d_1(x)d_2(x)}{\sigma_t(x,\tau)} \left(\left.\frac{\partial \sigma_t(K,\tau)}{\partial K}\right|_{K=x} \right)^2 \\
& \left. + \left.\frac{\partial^2 \sigma_t(K,\tau)}{\partial K^2}\right|_{K=x} \right],
\end{aligned}
$$

(5)

When considering such formulations, we also need to add non-arbitrage conditions to the state price density. We here follow the settings from [Brunner and Hafner, 2003], where for a friction-less and arbitrage-free market, and for a given maturity T, we need to have the following conditions:

1. Non-negativity property: The state price density is non-negative with $q(x) \geq 0$, $\quad x \geq 0$.

2. Integrability property: The state price density integrates to one, $\int_0^\infty q(x)\, dx = 1$.

3. Martingale property: The state price density reprices all calls, $\int_0^\infty \max\{x - K, 0\} q(x)\, dx = e^{r\tau} C_t(K,\tau)$, $\quad K \geq 0$.

3.1 Adaptive Local Quadratic Estimator for Implied Volatility

Following [Benko et al., 2007], we first deal with the observed IV from the market and try to give the estimation of true IV and its derivatives that removes noise. One can assume that the observed IV consists of true IV and some noise: $\tilde{\sigma}_i = \sigma\left(K_i\right) + \varepsilon_i$, where $\sigma\left(K_i\right)$ is true IV and $\tilde{\sigma}_i$ is the observed IV, i stands for the index of observed strikes, and ε_i is some unknown noise of IV on that specific strike. The local quadratic estimator $\hat{\sigma}(K)$ can be obtained by solving the following optimization problem:

$$\min_{\alpha_0,\alpha_1,\alpha_2} \sum_{i=1}^{n_\tau} \left\{ \tilde{\sigma}_i - \alpha_0 - \alpha_1\left(K_i - K\right) - \alpha_2\left(K_i - K\right)^2 \right\}^2 \mathcal{K}_h\left(K - K_i\right),$$

Here, $\mathcal{K}_h\left(K - K_i\right) \stackrel{\text{def}}{=} \frac{1}{h}\mathcal{K}\left(\frac{K - K_i}{h}\right)$ is a kernel function with bandwidth h. For example, $\mathcal{K}(u) = \frac{3}{4}\left(1 - u^2\right) I(|u| \leq 1)$ is used in [Benko et al., 2007], and it is known as a Epanechnikov kernel. Using Taylor expansion, it can be derived that:

$$\alpha_0 = \hat{\sigma}\left(K\right), \quad \alpha_1 = \hat{\sigma}'\left(K\right), \quad 2\alpha_2 = \hat{\sigma}''\left(K\right),$$

4

where $\hat{\sigma}(K)$ is the estimation for the true IV $\sigma(K)$ for a given strike K.

After solving this nonlinear optimization problem, the state price density for given strike K and given maturity T with time-to-maturity τ can be written as:

$$\hat{q}(K) = F\sqrt{\tau}\varphi(d_1)\left\{\frac{1}{K^2\alpha_0\tau} + \frac{2d_1}{K\alpha_0\sqrt{\tau}}\alpha_1 + \frac{d_1 d_2}{\alpha_0}(\alpha_1)^2 + 2\alpha_2\right\},$$

As this might violate non-arbitrage condition for non-negative property, we also need to impose the following constraint:

$$F\sqrt{\tau}\varphi(d_1)\left\{\frac{1}{K^2\alpha_0\tau} + \frac{2d_1}{K\alpha_0\sqrt{\tau}}\alpha_1 + \frac{d_1 d_2}{\alpha_0}(\alpha_1)^2 + 2\alpha_2\right\} \geq 0,$$

where τ is the time to maturity, $F = Se^{r\tau}$ is the forward price, and φ is the probability density function of a standard normal random variable.

[Benko et al., 2007] uses a constant bandwidth and a fixed kernel which is Epanechnikov kernel, and [Fengler and Hin, 2015] extends this method by using a two-univariate spline kernel that can accommodates B-splines of any order. Nonetheless, The bandwidth choice for h also influences the final accuracy of the estimation significantly. Original local quadratic regression model manually choose a constant h for different market data and models, but this approach is highly heuristic and can be unstable if we have little prior information about the market data. One solution we give here is to choose an adaptive h that can cover sufficient neighbourhood observations: since K_h is nonnegative within the (localization) window $[K - h, K + h]$, points outside of this interval have no influence on the estimator $\hat{\sigma}(K)$. In this sense, we can choose the number of points to be included in the localization window instead of the bandwidth h. This approach leads to more stable outcomes, particularly when there are insufficient observations near the boundary of the strike. Adding more observation points in these extreme cases can achieve the same level of estimation accuracy as in regions with abundant neighboring points.

3.2 Log-normal Approximation for Marginal Tails

In section 3.1 we impose the non-negative arbitrage-free condition. Following [Brunner and Hafner, 2003], in this section we impose the remaining two conditions **2&3** by modeling tails of the state price density. We treat our state price density function as a piecewise function:

$$q(x; \theta_L, \theta_U) = \begin{cases} q^L(x; \theta_L), & x < K_L, \\ q^{\mathcal{M}}(x), & K_L \leq x \leq K_U, \\ q^U(x; \theta_U), & x > K_U, \end{cases}$$

Here L, U stand for the lower and upper bounds of observed strikes, θ_L, θ_U are the parameters for the respective left-tail and right-tail state price density; $\mathcal{M} = [K_L, K_U]$. The remaining two constraints can be shown to be equivalent to the following relations:

$$\int_0^{K_L} q^L(x; \theta_L)\,\mathrm{d}x + \int_{K_U}^\infty q^U(x; \theta_U)\,\mathrm{d}x = 1 - \int_{K_L}^{K_U} q^{\mathcal{M}}(x)\mathrm{d}x, \tag{6}$$

$$-\,\mathrm{e}^{r\tau}\frac{\partial C_t^{\mathcal{M}}(K, \tau)}{\partial K}\bigg|_{K=K_U} = \int_{K_U}^\infty q(x; \theta_L, \theta_U)\,\mathrm{d}x, \tag{7}$$

$$1 + \mathrm{e}^{r\tau}\frac{\partial C_t^{\mathcal{M}}(K, \tau)}{\partial K}\bigg|_{K=K_L} = 1 - \int_{K_L}^\infty q(x; \theta_L, \theta_U)\,\mathrm{d}x, \tag{8}$$

$$F_t(\tau) = \int_0^{K_L} xq^L(x; \theta_L)\,\mathrm{d}x + \int_{K_L}^{K_U} xq^{\mathcal{M}}(x)\mathrm{d}x + \int_{K_U}^\infty xq^U(x; \theta_U)\,\mathrm{d}x, \tag{9}$$

where $F_t(\tau)$ is the forward price.

Assuming that the tail state price density is a mixture of two log-normal distributions, namely:

$$q^i(x; \theta_i) = \lambda_i \ell(x; \eta_{i,1}, v_{i,1}^2) + (1 - \lambda_i)\ell(x; \eta_{i,2}, v_{i,2}^2), \quad \lambda_i \in [0, 1], i \in \{L, U\},$$

where the lognormal density function is defined as:

$$\ell(x; \eta_{i,j}, v_{i,j}^2) = \frac{1}{xv_{i,j}\sqrt{2\pi}}\exp\left(-\frac{1}{2}\left(\frac{\ln(x) - \ln(\eta_{i,j}) + \frac{v_{i,j}^2}{2}}{v_{i,j}}\right)^2\right), \quad j = 1, 2; i \in \{L, U\},$$

and $\theta_i = (\lambda_i, \eta_{i,1}, v_{i,1}^2, \eta_{i,2}, v_{i,2}^2)'$ for $i \in \{L, U\}$. Here we impose the boundary condition for the derivatives of IV, that is:

$$\left.\frac{\partial q^L(x; \theta_L)}{\partial x}\right|_{x=K_L} = \left.\frac{\partial q^{\mathcal{M}}(x)}{\partial x}\right|_{x=K_L} \quad \text{and} \quad \left.\frac{\partial q^U(x; \theta_U)}{\partial x}\right|_{x=K_U} = \left.\frac{\partial q^{\mathcal{M}}(x)}{\partial x}\right|_{x=K_U},$$

The intuition that we impose the derivative boundary condition is to guarantee the smoothness condition, which later facilitates us to obtain the optimality of the Trapezoidal Rule Scheme in Bass-LV calibration process.

The ten-parameter, nonlinear system can be reduced to a nonlinear equation with one parameter, which can be solved numerically by standard one-dimensional root-finding methods. Details can be seen in [Brunner and Hafner, 2003], and the relationships between parameters are:

$$N(z_i) = N(d_2(K_i)) - K_i n(d_2(K_i)) \sqrt{\tau} \left.\frac{\partial \sigma_t(K, \tau)}{\partial K}\right|_{K=K_i}, i \in \{L, U\}, \tag{10}$$

$$\lambda_i = \frac{q^{\mathcal{M}}(K_i) - \frac{1}{K_i v_{i,2} \sqrt{2\pi}} e^{-\frac{1}{2} z_i^2}}{\frac{1}{K_i v_{i,1} \sqrt{2\pi}} e^{-\frac{1}{2} z_i^2} - \frac{1}{K_i v_{i,2} \sqrt{2\pi}} e^{-\frac{1}{2} z_i^2}}, \tag{11}$$

$$\eta_{i,1} = K_i e^{z_i v_{i,1} + \frac{v_{i,1}^2}{2}}, \quad \eta_{i,2} = K_i e^{z_i v_{i,2} + \frac{v_{i,2}^2}{2}}, \tag{12}$$

$$v_{i,1} = \frac{q^{\mathcal{M}}(K_i) - \frac{1}{K_i v_{i,2} \sqrt{2\pi}} e^{-\frac{1}{2} z_i^2}}{\left(q^{\mathcal{M}}(K_i) + K_i \left.\frac{\partial q^{\mathcal{M}}}{\partial x}\right|_{x=K_i}\right) \frac{1}{z_i} - \frac{q^{\mathcal{M}}(K_i)}{v_{i,2}}}, \tag{13}$$

$$\lambda_L \eta_{L,1} N(-z_L - v_{L,1}) + (1 - \lambda_L) \eta_{L,2} N(-z_L - v_{L,2})$$
$$= F_t(\tau) N(-d_1(K_L)) + K_L^2 n(d_2(K_L)) \sqrt{\tau} \left.\frac{\partial \sigma_t(K, \tau)}{\partial K}\right|_{K=K_L}, \tag{14}$$

$$\lambda_U \eta_{U,1} N(z_U + v_{U,1}) + (1 - \lambda_U) \eta_{U,2} N(z_U + v_{U,2})$$
$$= F_t(\tau) N(d_1(K_U)) - K_U^2 n(d_2(K_U)) \sqrt{\tau} \left.\frac{\partial \sigma_t(K, \tau)}{\partial K}\right|_{K=K_U}, \tag{15}$$

$n(\cdot)$ stands for the p.d.f of a standard normal random variable. The reason to choose two lognormal approximation is that a single lognormal assumption for tail distribution is not enough to solve the equations system 6 to 9 and avoid the arbitrage condition. Furthermore, to prevent calendar arbitrage between options of different maturities, we impose a condition that ensures the state price densities for different maturities satisfy:

$$\int_0^\infty \max\{x - K, 0\} \left(e^{r(T_{i+1} - T_i)} q_{S_{T_{i+1}}}(x) - q_{S_{T_i}}\left(x e^{-r(T_{i+1} - T_i)}\right)\right) dx \geq 0, \tag{16}$$

for all maturities $T_i \leq T_{i+1}$, where T_is are some maturities in our market observations.

4 Optimality and Convergence Rate of Numerical Convolution

In this section, we demonstrate the optimality and convergence rates of the Trapezoidal Rule Scheme under worst-case scenarios for numerical convolution of Bass-LV implementation. "Worst case" pertains to conditions of limited smoothness in marginal distribution functions and their inverses. This arises in our numerical implementation, where spline interpolation and extrapolation are utilized to approximate the implied distribution functions and their inverses.

Recall the fixed-point algorithm:

$$\mathcal{A}F := F_{\mu_i} \circ \left(K_{T_{i+1} - T_i} \star \left(F_{\mu_{i+1}}^{-1} \circ \left(K_{T_{i+1} - T_i} \star F\right)\right)\right).$$

Lemma 2.2 in [Conze and Henry-Labordere, 2021] shows that $\mathcal{A}(\mathcal{E}) \subset \mathcal{E}$, where $\mathcal{E}$ is the space of cumulative distributions (i.e., non-decreasing right-continuous functions $F : \mathbb{R} \to [0, 1]$ with $\lim_{x \to -\infty} F(x) = 0$ and $\lim_{x \to \infty} F(x) = 1$). Consequently, in each iteration of the fixed-point algorithm, we will obtain a well-defined cumulative probability function (CDF).

Following Theorem 2.4 in [Conze and Henry-Labordere, 2021], we have that $\mathcal{A}(\mathcal{E})$ is uniformly bounded and Lipschitz, which implies, by the Arzelà-Ascoli theorem, that $\mathcal{A}$ is continuous in the sup-norm and $\mathcal{A}(\mathcal{E})$ is relatively compact. Additionally, $\mathcal{E}$ is convex, closed, and $\mathcal{A}(\mathcal{E}) \subset \mathcal{E}$. By Schauder's fixed point theorem, a fixed point $\bar{F} \in \mathcal{E}$ exists.

Now, consider a sequence F_n in $\mathcal{E}$ that converges to F in the sup-norm. Since F_n and F are distribution functions, they are bounded. Sup-norm convergence means that for any $\epsilon > 0$, there exists an N such that for all $n > N$, $\sup_{x \in \mathbb{R}} |F_n(x) - F(x)| < \epsilon$ which implies that for all $x \in \mathbb{R}, |F_n(x) - F(x)| < \epsilon$. Therefore, $\mathcal{A}F_n$ converges to $\mathcal{A}F$ in the sup-norm as well.

In numerical implementation, interpolation/extrapolation is needed for representing the unknown distribution function. Therefore, without loss of generality, we assume that the original unknown distribution function can be sufficiently approached by interpolation/extrapolation with enough data points. For simplicity, we also assume that properties like aforementioned continuous property will hold through the fixed-point algorithm, and assume that the error terms caused by information loss in the iteration process are negligible.

Assuming we have N maturities, and F_{μ_i} stands for the marginal distribution for i^{th} maturity, we can have the following:

Corollary 1. *Given analytic functions F_{μ_i}, $F_{\mu_i}^{-1}$, $F_{\mu_i}^{-1} \neq F_{\mu_{i+1}}^{-1}$, $\forall i \in \{1, 2, \cdots, N-1\}$, the analytic property holds for converged result $F_{W_{T_i}}$. In particular, when marginal distribution follows lognormal distribution(e.g. Black-Scholes model), $F_{W_{T_i}}$ shows analytic property except at the boundary. In addition, given functions F_{μ_i}, $F_{\mu_i}^{-1}$ with some smoothness order, smoothness property holds for converged result $F_{W_{T_i}}$.*

Given two consecutive maturities T_1, T_2 in fixed-point algorithm, the following multi-layer integration needs to be done to compute the CDF $F_{W_{T_1}}(w)$:

$$
K_{T_2-T_1} * F_{\mu_2}^{-1} \left(K_{T_2-T_1} * F_{W_{T_1}}(w) \right) = \int_{-\infty}^{\infty} \rho(y) * F_{\mu_2}^{-1} \circ g(w - y)\, dy
$$

$$
= \int_{-\infty}^{\infty} \rho(y) * F_{\mu_2}^{-1} \left(K_{T_2-T_1} * F_{W_{T_1}}(w - y) \right)\, dy
$$

$$
= \left(\int_{-\infty}^{\infty} \rho(y) * F_{\mu_2}^{-1} \left(\int_{-\infty}^{\infty} F_{W_{T_1}}(w - y - x)\rho(x)\, dx \right)\, dy. \right) \tag{17}
$$

where $\rho(\cdot)$ is given by the heat kernel $K_{T_2-T_1}$, $g := K_{T_2-T_1} * F_{W_{T_1}}$.

With this expression, we can derive the following convergence rate for Gauss-Hermite quadrature in Bass-LV:

Corollary 2. *Both internal and external integrand in Eq17 are well-defined in following weighted Sobolev space*

$$
\mathscr{H}_m := \left\{ f \in L_\rho^2 \mid \|f\|_m := \left(\sum_{\tau=0}^{m} \left\| f^{(\tau)} \right\|_{L_\rho^2}^2 \right)^{1/2} < \infty \right\}
$$

where $m \in \mathbb{N}$, $\rho(x) = \frac{1}{\sqrt{2\pi\sigma^2}} e^{-\frac{x^2}{2\sigma^2}}$, $f^{(\tau)} \in L_\rho^2$ for $\tau = 1, \ldots, m$, and $L_\rho^2 := L_\rho^2(\mathbb{R})$. The convergence rate of Gauss-Hermite quadrature for one integrand can achieve $\mathcal{O}\left(n^{-m/2} \right)$, where the n stands for the number of quadrature points, m stands for the order of smoothness for selected integrand.

In the following, we deal with the optimal parameter settings for Trapezoidal Rule Scheme in Bass-LV implementation, and give the convergence rate for integrand in corresponding numerical convolution. We first write the Trapezoidal Rule Scheme as follows:

$$
\text{Integration} = \sum_{m=-M}^{M} \rho(mh) * F_{\mu_2}^{-1} \left(\sum_{n=-N}^{N} F_{W_{T_1}}(w - mh - nh)\rho(nh)h \right) * h, \tag{18}
$$

where h is step size, M and N represent the number of terms used in the Trapezoidal Rule Scheme.

Following the idea of proposition 4.2 in [Kazashi et al., 2023], We can derive the optimality for the inner and outer parts respectively:

Proposition 1. *Denote that the inner integrand in Bass-LV implementation has the smoothness of order m, $\epsilon \in (max\{1 - \sigma^2, 0\}, 1)$, and $\sigma^2 = T_{i+1} - T_i$ for the integrand computing converged result $F_{W_{T_i}}$. We can obtain the optimal parameter settings for the inner integrand as:*

$$
Mh = \sqrt{\frac{2(T_{i+1} - T_i)}{(1 - \epsilon)} m \ln(2M + 1)},
$$

$$
h = \frac{\sqrt{\frac{2(T_{i+1} - T_i)}{(1 - \epsilon)} m \ln(2M + 1)}}{M}.
$$

Optimality above holds true for outer integrand on Nh, h by imposing outer integrand smoothness order and independently chosen $\epsilon \in (max\{1 - \sigma^2, 0\}, 1)$. Under these optimal settings, one can achieve the convergence rate of Trapezoidal Rule Scheme for one integrand as $\mathcal{O}\left(\frac{(\ln n)^{(m/2+1/4)}}{n^m}\right)$ in Bass-LV implementation, where m represents the smoothness order for that integrand, and n represents the terms used in trapezoidal rule.

We can conclude that, when compared under the same part of integrand, same number of points used, and same order of smoothness m, the convergence rate of Trapezoidal Rule Scheme as $\mathcal{O}\left(\frac{(\ln n)^{(m/2+1/4)}}{n^m}\right)$ is faster than that of the Gauss Hermite $\mathcal{O}\left(n^{-m/2}\right)$. This gives the theoretical foundation for faster convergence speed in Trapezoidal Rule Scheme when have sufficient points used compared to Gauss-Hermite quadrature.

5 Numerical Results

5.1 Step-by-Step Calibration Procedure

In this section, we outline a step-by-step procedure for calibrating the Bass-LV model from European vanilla options market data.

1. **Extract implied volatilities (IV) from market prices:** Begin with observed market prices of European vanilla options. Compute the implied volatilities for different strikes and maturities.

2. **Fit a local quadratic regression model:** Use the extracted IVs to fit a local quadratic regression (LQR) model. This involves solving the following optimization problem to estimate the parameters α_0, α_1, and α_2:

$$\min_{\alpha_0, \alpha_1, \alpha_2} \sum_{i=1}^{n_\tau} \left\{\tilde{\sigma}_i - \alpha_0 - \alpha_1 \left(K_i - K\right) - \alpha_2 \left(K_i - K\right)^2\right\}^2 \mathcal{K}_h \left(K - K_i\right),$$

   where $\mathcal{K}_h$ is a kernel function with bandwidth h.

3. **Calculate the state price density:** Using the parameters α_0, α_1, and α_2 from the LQR model, compute the state price density $q^{\mathcal{M}}(x)$ on the interval $\mathcal{M} = [K_L, K_U]$ as follows:

$$q^{\mathcal{M}}(x) = F\sqrt{\tau}\varphi\left(d_1\right) \left\{\frac{1}{x^2\alpha_0\tau} + \frac{2d_1}{x\alpha_0\sqrt{\tau}}\alpha_1 + \frac{d_1 d_2}{\alpha_0}\left(\alpha_1\right)^2 + 2\alpha_2\right\},$$

   Here, K_L and K_U refer to the minimum and maximum observed strikes from the market data, respectively. After completing this step, one obtains the portion of the state price density corresponding to the market observations.

4. **Construct the tails of the state price density:** Use mixture of lognormal distributions to construct tails of the state price density. This can be achieved by leveraging the parameters obtained in the previous step and then by solving the root-finding system in section 3.2. After completing this step, one obtains the state price density on $[0, K_L]$ and $[K_U, \infty]$.

5. **Complete the state price density:** Combine the densities from the steps above to form a complete state price density $q(x; \theta_L, \theta_U)$:

$$q(x; \theta_L, \theta_U) = \begin{cases} q^L(x; \theta_L), & x < K_L \\ q^{\mathcal{M}}(x), & K_L \leq x \leq K_U \\ q^U(x; \theta_U), & x > K_U \end{cases}.$$

6. **Calibrate the Bass-LV model:** With the arbitrage-free state price densities and corresponding marginal distributions obtained above as input, using trapezoidal numerical convolution, solve the fixed-point problem to perform the calibration. It involves iteratively calculating the following:

$$\mathcal{A}F := F_{\mu_i} \circ \left(K_{T_{i+1}-T_i} \star \left(F_{\mu_{i+1}}^{-1} \circ \left(K_{T_{i+1}-T_i} \star F\right)\right)\right)$$

   until convergence is achieved. Details can be seen in section 3.4 of [Conze and Henry-Labordere, 2021].

This step-by-step procedure provides a structured approach to calibrate the Bass-LV model.

5.2 Iteration and Calibration Errors

In the Bass construction, a fix-point problem needs to be solved iteratively. Following the practice in [Conze and Henry-Labordere, 2021], the stopping condition is specified by controlling the following iteration error measured in the infinite norm:

$$err_{itr} = \left\| F_{W_{T_i}}^{(p)} - F_{W_{T_i}}^{(p-1)} \right\|_\infty.$$

The iteration continues until the iteration error is less than a predetermined tolerance level. The iteration error tolerance naturally determines the quality of calibration. Let err_{cab} be the calibration error, which is the mean absolute percentage error of calibrated IV:

$$err_{cab} = \frac{1}{L} \sum_{j=1}^{L} \left| \frac{IV_{cab}^j - IV_{True}}{IV_{True}} \right|.$$

Here L is the number of option strike prices considered. In the following experiments, we numerically investigate how calibration error depends on iteration error tolerance.

5.3 Experiments in the Black-Scholes-Merton Case

In this section, we examine the Bass-LV calibration in the Black-Scholes-Merton model. In this case, the marginal distributions and their inverse are known and hence do not introduce any implementation error. The exact solution of the fixed point problem is also available in closed-form. This allows us to examine how iteration error control in numerical solution of the fixed point problem impacts calibration performance. It also enables us to compare different integration schemes and highlight the advantages of trapezoidal numerical convolution.

Let μ_1, μ_2 and μ_3 be lognormal distributions, where the standard deviations of the corresponding normal distributions are $\sigma\sqrt{T_1}, \sigma\sqrt{T_2}$ and $\sigma\sqrt{T_3}$, respectively . In this case, the solution to the fixed point problem is $F_{W_{T_i}} = \mathcal{N}\left(\frac{\cdot}{\sqrt{T_i}}\right)$ and $f(t, w) = S_0 \exp\left(-\frac{1}{2}\sigma^2 t + \sigma w\right)$.

In our experiment, the current time is $T_0 = 0$. Options with the following maturities are considered: $T_1 = 1, T_2 = 1.2$ and $T_3 = 1.5$. The initial asset price is $S_0 = 100$, the true IV is $\sigma = 1$, and the risk-free interest rate is $r = 0$. The details of the experiment are given below:

Algorithm 1 The Black-Scholes-Merton Case

Step 1: Given the lognormal marginal distributions: $S_{T1} \sim \mu_1, S_{T2} \sim \mu_2, S_{T3} \sim \mu_3$
Step 2: Numerically solve the fixed-point problem to get $F_{W_{T_i}}$
Step 3: Simulate the spot price process and estimate European call option prices
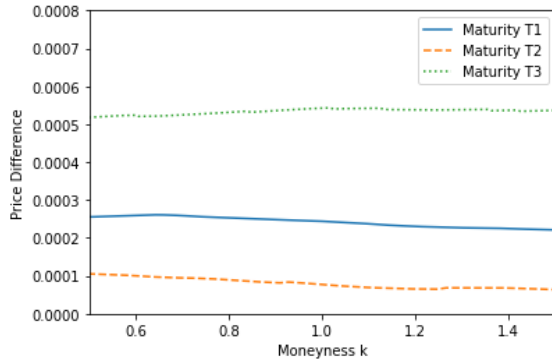Step 4: Compute the IVs associated with the above call prices and compare to the true IV

Figure 3: Pricing errors of options with maturities $T_1 = 1, T_2 = 1.2, T_3 = 1.5$ and moneyness $k = K/S_0$ in the calibrated Bass-LV model. Iteration error tolerance $= 10^{-5}$.
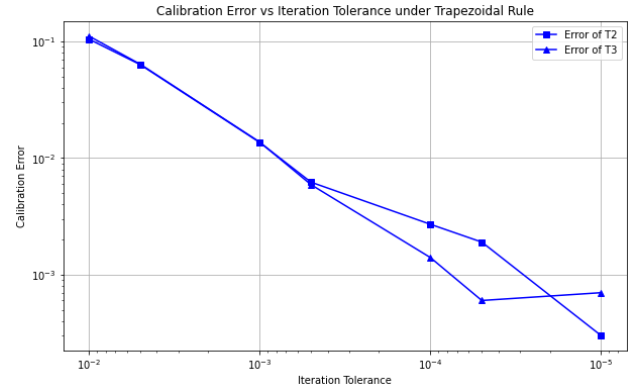
Figure 4: MAPE of calibrated implied volatility in the Black-Scholes-Merton case. Trapezoidal rule used for numerical integration.

Figure 3 shows that the absolute pricing errors of European call options with the above three maturities and various strikes are bounded by 6×10^{-4} in the calibrated model. Here, we consider option strike prices that are in $[0.5S_0, 1.5S_0]$.
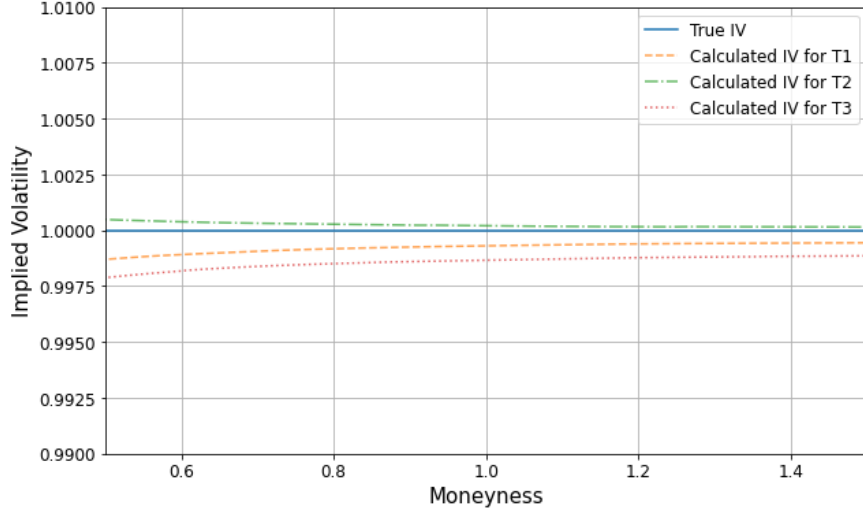
Figure 5: Calibrated IV in the Black-Scholes-Merton case for maturities $T_1 = 1$, $T_2 = 1.2$, $T_3 = 1.5$ and moneyness $k = K/S_0$.

Options with these strikes are most actively traded. Figure 5 shows that the implied volatilities of the above options in the calibrated Bass-LV model are very close to the true IV, which is 1.

Iteration error tolerance in Figures 3 and 5 is set to 10^{-5}, i.e, the fixed point algorithm will stop when $\left\| F_{W_{T_i}}^{(p)} - F_{W_{T_i}}^{(p-1)} \right\|_\infty \leq 10^{-5}$ for some iteration index p.

In Figure 4, we show the numerical relationship between iteration error tolerance and calibration error. European option prices are computed using Monte Carlo simulation with sample size 3×10^8. Calibrated IVs are then computed from these estimated option prices. When plotting err_{cab}, we re-run the Monte Carlo method several times with different random seeds and plot the median err_{cab}. This is to mitigate the impact of noisy random number generators and show a clearer relationship between iteration error tolerance and calibration accuracy. Since no fixed point problem needs to be solved for options with maturity T_1, we didn't plot the error for this maturity.

As can be seen in Figure 4, as the iteration error tolerance decreases, calibration accuracy improves approximately linearly. In this particular example, to get a calibration error of 1%, an iteration error tolerance of about 10^{-3} is needed. In numerical experiments in [Conze and Henry-Labordere, 2021], an iteration error tolerance of 2×10^{-3} was used. However, when higher accuracy levels are desired in some applications, one must use a much smaller iteration error tolerance. For example, if the desired calibration error is 0.01%, an iteration error tolerance of 10^{-5} would be needed. In such cases, trapezoidal rule based numerical integration schemes clearly become more advantageous compared to the Gauss-Hermite quadrature, as to be shown next. Note that the calibration error for maturity T_3 flattens after reaching 10^{-3}. This is due to not large enough Monte Carlo sample size. Consequently, error due to Monte Carlo estimation starts to dominate. Increasing Monte Carlo sample size or using variance reduction techniques will help further reducing the calibration error.

Figure 6 compares the performance of Gauss-Hermite Quadrature and the Trapezoidal Rule under different iteration error tolerance settings. The horizontal axis is the minimal amount of time the numerical solution of the fixed point problem takes to achieve the smallest possible calibration accuracy. It shows that, as the iteration error tolerance decreases, the computational time required when using the trapezoidal rule becomes much smaller compared to Gauss Hermite Quadrature. This clearly shows the advantage of using the trapezoidal rule, in particular, when the desired accuracy level is high.

Our numerical results also support the linear convergence theory of the Bass calibration process presented in [Acciaio et al., 2023]. Figure 7 clearly shows that, for a given maturity, the number of iterations needed to solve the fixed point problem grows linearly in the logarithm of the iteration error tolerance. In later numerical experiments, we show that this is also roughly true in much more general settings than those specified in [Acciaio et al., 2023].

Tables 1 and 2 provide detailed results for the plots. These experiments were conducted using a 14th Gen Intel(R) Core(TM) i9-14900HX CPU @ 2.20 GHz and Python 3.11.9. All subsequent experiments are performed within this environment. The first column contains the iteration error tolerance. The second column contains the minimal amount
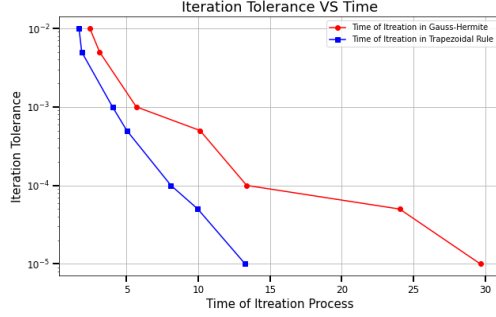
Figure 6: Time for Iteration Process with Different Tolerance using Two Numerical Schemes under the Black-Scholes Model
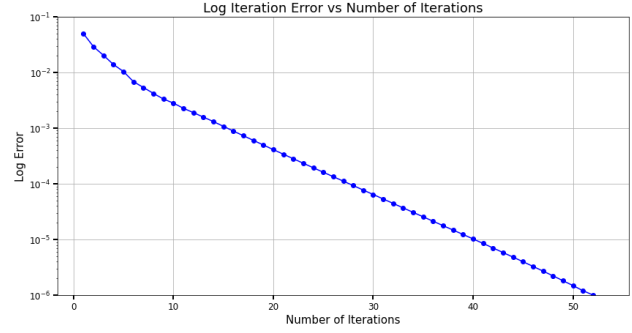

Figure 7: Iteration Tolerance vs. Iteration Numbers under the Black-Scholes Model

of time needed to solve the fixed point problem to achieve the smallest possible calibration error. For the third column, note that no fixed point problem is solved for the first maturity. The error here is totally due to Monte Carlo estimation. The last two columns contain the calibration errors for the remaining two maturities.

Table 1: Time and Error Outcomes for Gauss Hermite Quadrature under Black Scholes Model for Different Maturities

Iteration Tolerance	Iteration Time	Calibration Acc of T_1	Calibration Acc of T_2	Calibration Acc of T_3
1E-02	2.4	8.0E-04	1.1E-01	1.1E-01
5E-03	3.1	8.0E-04	6.7E-02	6.4E-02
1E-03	5.7	8.0E-04	1.3E-02	1.4E-02
5E-04	10.1	8.0E-04	7.2E-03	6.0E-03
1E-04	13.4	8.0E-04	2.3E-03	2.1E-03
5E-05	24.0	8.0E-04	1.0E-03	8.0E-04
1E-05	29.7	8.0E-04	3.0E-04	6.0E-04

Table 2: Time and Error Outcomes for Trapezoidal Rule Scheme under Black Scholes Model for Different Maturities

Iteration Tolerance	Iteration Time	Calibration Acc of T_1	Calibration Acc of T_2	Calibration Acc of T_3
1E-02	1.7	8.0E-04	1.0E-01	1.1E-01
5E-03	1.9	8.0E-04	6.3E-02	6.4E-02
1E-03	4.0	8.0E-04	1.4E-02	1.4E-02
5E-04	5.0	8.0E-04	6.2E-03	5.9E-03
1E-04	8.1	8.0E-04	2.7E-03	1.4E-03
5E-05	10.0	8.0E-04	1.9E-03	6.0E-04
1E-05	13.3	8.0E-04	3.0E-04	7.0E-04

5.4 Comparison with the Breeden-Litzenberger Approach

Generating the state price density is one of the most important steps in Bass LV calibration. In this section, we compare our proposed method with the widely used Breeden-Litzenberger formula. The Breeden-Litzenberger approach usually starts with cleaning and smoothing the market prices to meet non-arbitrage conditions. The state price density is then derived using the formula:

$$q(x) \stackrel{\text{def}}{=} e^{r\tau} \frac{\partial^2 C_t(K, \tau)}{\partial K^2}\bigg|_{K=x}.$$

To eliminate the need for the non-trivial price cleaning and smoothing step for the Breeden-Litzenberger approach, we generate arbitrage-free option prices and use them as "market" data. The experiment is done in the Stochastic Volatility Inspired (SSVI) model from [Gatheral and Jacquier, 2014]. Given the arbitrage-free option price surface generated in this model, we apply the Breeden-Litzenberger formula to derive the state price densities for different maturities using finite difference.

11

Our proposed method on the other hand is rather robust, even when market data contains noise. To numerically illustrate this, we add some random noise to the arbitrage-free SSVI surface. This produces a pseudo-market IV surface with potential arbitrage. We then apply our proposed method to generate state price densities and corresponding marginal distributions for different maturities. The following is an outline of the proposed method:

Algorithm 2 The SSVI Case

Step 1: Generate "market" data from the SSVI model. Add random noise. Apply the LQR method to construct the central part of the state price density.
Step 2: Use lognormal mixture to construct the tails of the state price density.
Step 3: Numerically solve the fixed-point problem to get $F_{W_{T_i}}$
Step 4: Simulate the spot price process and estimate European call option prices
Step 5: Compute the IVs associated with the above call prices and compare to the true IV.

Recall that for the Heston-like SSVI model presented in [Gatheral and Jacquier, 2014], the function φ is defined as:

$$\varphi(\theta_t) = \frac{1}{\lambda\theta_t}\left\{1 - \frac{1 - e^{-\lambda\theta_t}}{\lambda\theta_t}\right\},$$

where $\lambda \geq \frac{(1+|\rho|)}{4}$ ensures no arbitrage. In this model, the state price density can be computed analytically. This allows us to examine the quality of the state price densities estimated using the proposed method and the Breeden-Litzenberger approach. More specifically, the total variance surface is given by:

$$w(k, \theta_t) = \frac{\theta_t}{2}\left\{1 + \rho\varphi(\theta_t)k + \sqrt{(\varphi(\theta_t)k + \rho)^2 + (1 - \rho^2)}\right\}.$$

The corresponding IV surface is then obtained via

$$\sigma(k, t) = \sqrt{\frac{w(k, \theta_t)}{t}}, \tag{19}$$

where k represents log moneyness, i.e.

$$e^k = \frac{K}{S_0 e^{r\tau}}$$

with τ being the time to maturity and K the strike price. By computing σ, σ', σ'' and using equation 5 we can obtain the closed-form expression for the true state price density to serve as a benchmark.

For our experiment, we set the parameters as follows: $\rho = 0.3$, $\lambda = \frac{(1+|\rho|)}{4} + 1$, and $\theta_t = 0.4t$. The initial spot price is set at $S_0 = 100$. The risk-free rate is $r = 0$. Figure 8 illustrates the resulting SSVI surface. Suppose the first option maturity to be considered is $T_1 = 2$. Given the previously generated IVs with random noise, Figure 9 presents the recovered IVs using local quadratic regression (LQR). Despite the presence of noise and potential arbitrage in the inputs, the LQR method effectively recovers the true IV with great accuracy. From IVs calibrated using local quadratic regression, we construct the lognormal mixture tails. Table 3 shows the parameters obtained, where K_L and K_U represents the minimal and maximal observed strike prices. Figure 10 shows the corresponding estimated state price density with lognormal mixture tails.

Table 3: Parameters for Lognormal Mixture Tails

Parameter	Lower (i=L)	Upper (i=U)
λ_i	0.879196378130754	0.02134579716024674
$v_{i,1}$	0.9999323268888954	0.13848417203576707
$v_{i,2}$	0.696842788545524	0.9465074896268826
$\eta_{i,1}$	1.5907735996100631	1.3991088947706756
$\eta_{i,2}$	0.5304563920216386	0.9420478564063081
K_i	6.016806722689075	159.8655462184874

To compare to the Breeden-Litzenberger approach, we consider a range of $[6, 160]$ for the strike price. For the Breeden-Litzenberger approach, spline interpolation and extrapolation are used, with boundary conditions ensuring well-defined extrapolations. To optimize the performance of the Breeden-Litzenberger method, we use 120 evenly spaced strike
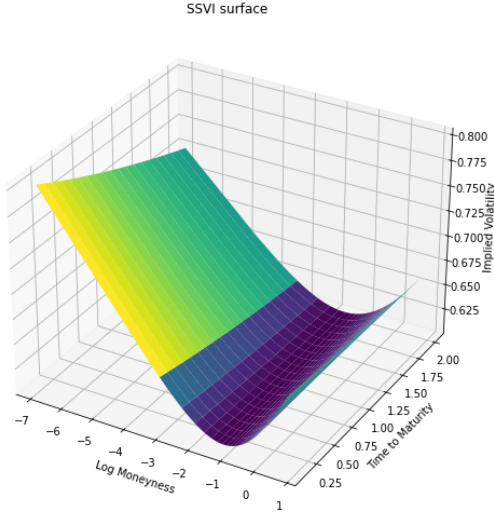
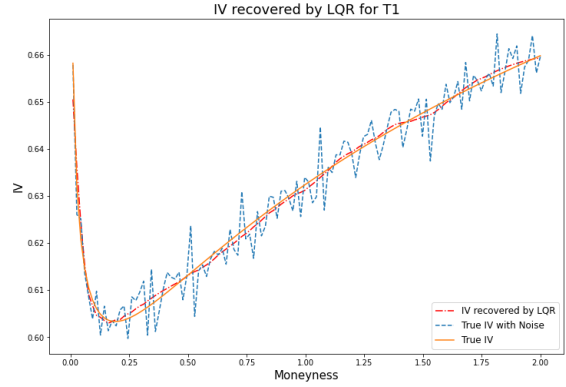Figure 8: Heston-like SSVI implied volatility surface

Figure 9: IVs recovered by Loacl Quadratic Regression for maturity T_1 from data with noise
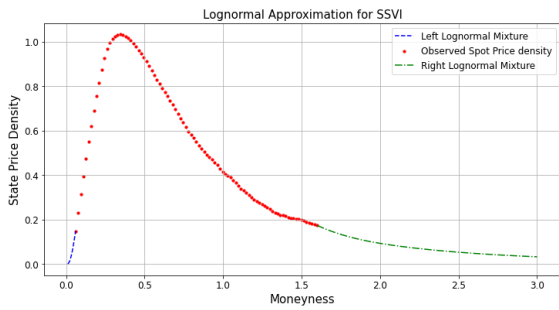

Figure 10: Estimated state price density with lognormal-mixture tails from data with noise
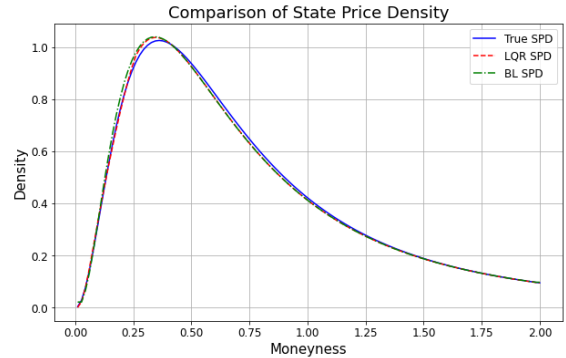

Figure 11: Estimated state price density: proposed method vs Breeden-Litzenberger

prices ranging from 5 to 200, since the performance of the Breeden-Litzenberger method relies heavily on the accuracy of finite difference, which requires a larger number of observations.

Under these settings, we compare the two approaches in Figures 11, 12, and 13. In Figure 11, "LQR SPD" shows the state price density constructed using our proposed approach with local quadratic regression and lognormal mixture tails. "BL SPD" represents the state price density constructed using the Breeden-Litzenberger method. "True SPD" represents the true state price density in the Heston-like SSVI model.

Although both "LQR SPD" and "BL SPD" seem to be close to the true state price density, our proposed method provides a much more accurate estimation. Figure 12 shows the absolute error for both estimated state price densities. It can be seen that the proposed method (dashed line) achieves better accuracy compared to the Breeden-Litzenberger method (solid line). The latter shows notable errors for moneyness below 0.25 or above 2. This leads to much larger errors for calibrated implied volatilities. In Figure 13, we compare the implied volatilities (IVs) obtained from both methods to true IVs (represented by the dash-dotted line). The solid curve, generated using the Breeden-Litzenberger method, deviates significantly from the true IV. In contrast, IVs calculated using our proposed method (represented by the dashed line) closely aligns with the true IV.

5.5 Numerical Experiment Based on TSLA Market Data

We conduct an experiment using the TSLA market smile data from July 1st, 2020. Since TSLA does not pay dividends, we adjust the data to treat call options as vanilla options by regularizing the risk-free rate. The three maturities we select
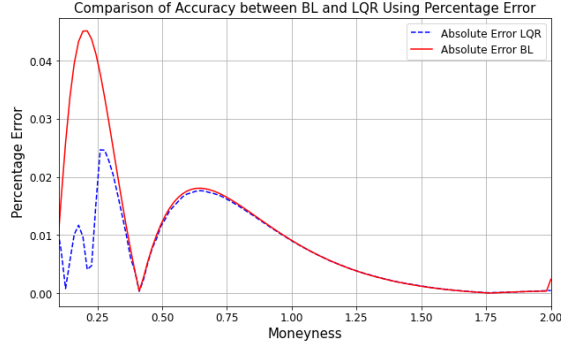
Figure 12: Estimation error for state price density: proposed method vs Breeden-Litzenberger
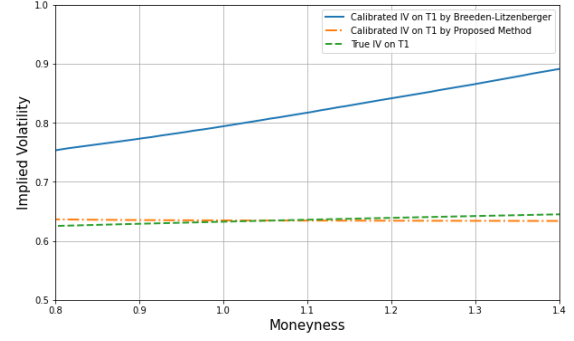

Figure 13: Calibrated IV: proposed method vs Breeden-Litzenberger

are 2020/09/18, 2020/10/16, and 2021/01/15, when sufficient market observations were available for call options. The option data is sourced from OptionMetrics.

Since the Bass construction assumes a zero interest rate, the data needed to be regularized accordingly. Assuming the starting maturity is $T_0 = 0$, the forward price at time t is given by $F(t) = S_0 e^{rt}$. We define the moneyness at time t as $km(t) = \frac{K_t}{F(t)}$ where $K(t)$ is the real strike on time t. As such, The normalized call option price is calculated as:

$$C_N(t, km(t)) = \frac{C(t, K(t))}{F(t)}.$$

To avoid potential artificial jumps in implied volatility (IV) at the at-the-money (ATM) region, we applied a smoothing procedure to the IV curves. We use a blending approach as described in [Birru and Figlewski, 2010] and [Alexiou et al., 2023]. In this approach, the IVs of put and call options with strike prices within a specified range close to the underlying spot price S_0 are blended as follows:

$$\hat{IV}(K) = wIV_{put}(K) + (1 - W)IV_{call}(k)$$

with $w = \frac{K_{max} - K}{K_{max} - K_{min}}$, and $K_{max(min)}$ is the maximum(minimum) of strike price in that range. For our experiment, we focus on constructing the market smile on the call option side and comparing the results with market observations, choosing the blending region as $(0.5S_0, S_0)$. Result of smoothing for maturity T1 is shown in figure 14, and same for maturity T2,T3.

After cleaning and processing the data, we apply the LQR model to the three maturities to generate a non-arbitrage IV curve and corresponding discrete state price density observations. The fitted IV curve for maturity T1 is shown in figure 15, and same for maturity T2,T3.
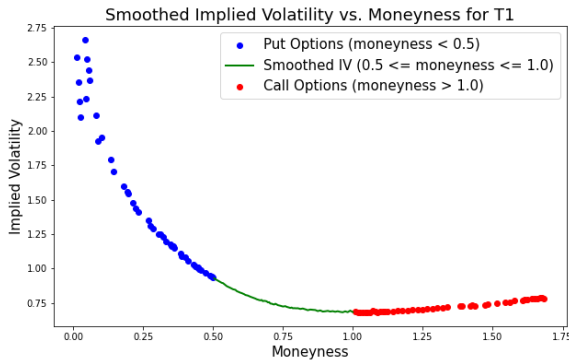

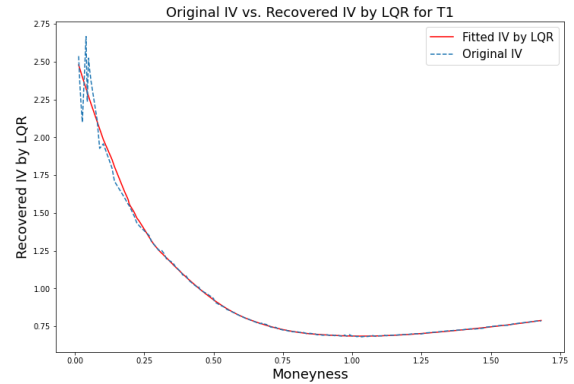Figure 14: Smoothed IV on Maturity T1

Figure 15: LQR Fitting for Maturity T1

Table 4 presents the parameter fitting results of the lognormal mixture approximation for three maturities. In the observed market data, there is notable trading activity in the small moneyness region ($0 < moneyness < 0.2$). This

leads to a market-specific phenomenon where the state price density exhibits an unusual pattern: it increases sharply near zero, dips to zero in its immediate vicinity, and then rises again. However, the lognormal mixture model assumes that the state price density should exhibit a monotonically decreasing trend at the strike boundaries. To satisfy this smoothness condition, the first-order derivative of the state price density with respect to strike prices must be positive at the left boundary and negative at the right boundary.

A common and safe approach to address this phenomenon is to "discard" the data, as it intuitively contradicts expectations for typical market transactions. For reference, in the SSVI experiment, the state price density follows a more expected "bell-shaped" curve. However, using the two-lognormal mixture model, we can also capture this specific anomaly to cater to potential specialized requirements.

Our strategy is as follows: we impose constraints on the lognormal mixture model, with $v_{L,1} \geq 1$, $v_{L,2} \in (0,1)$, and $\lambda_L > 0.5$. These constraints introduce a small peak near zero, while still maintaining the overall smoothness condition. The lower bound can be customized for various financial assets to achieve more precise fitting. Generally, setting the lower boundary for $v_{L,1}$ at 1 is sufficient to yield satisfactory simulation outcomes in the Bass-LV model, as demonstrated later in this experiment.

We use maturity T_1 as an example to illustrate the fitting results of the lognormal mixture approximation. The blue (red) line in Figure 16 represents the fitted lognormal mixture curve, superimposed on a limited region of observed market data for the state price density. The black points correspond to the market observations generated by the tuned LQR model. When constructing the approximation using a mixture of lognormal distributions, it is necessary to select a strike value near zero, with a positive derivative, to ensure a feasible solution. Although not all information from the black points near zero is utilized, the fitted lognormal mixture accurately captures the key characteristics of the state price density. This is evidenced by the close alignment of the blue curve with the black points in figure 16. For a more comprehensive view of the entire distribution, refer to figure 17, which provides detailed visualizations of the two-lognormal mixture structure.

Table 4: Parameter settings for lognormal mixture model

| Parameter	T1	T2	T3
λ_L	0.891814729	0.730072506	0.999997865
v_{L1}	11.83540063	35.27086006	5.874220433
v_{L2}	0.389034015	0.442752001	0.117462989
η_{L1}	3.476e+41	5.241e+302	348318051406
η_{L2}	0.789509660	0.946324794	0.289462222
λ_U	0.818069793	0.927681918	0.971590088
v_{U1}	0.283361639	0.345919720	0.437880299
v_{U2}	1.167721500	1.708909349	2.078893403
η_{U1}	1.027194390	0.994822411	1.004198445
η_{U2}	0.483430523	0.540870790	1.237646035
L_{cdf}	0.011757319	0.015447680	0.033174055
U_{cdf}	0.957228077	0.929827574	0.870975267
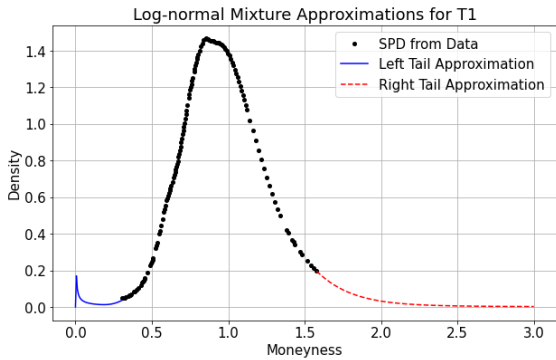
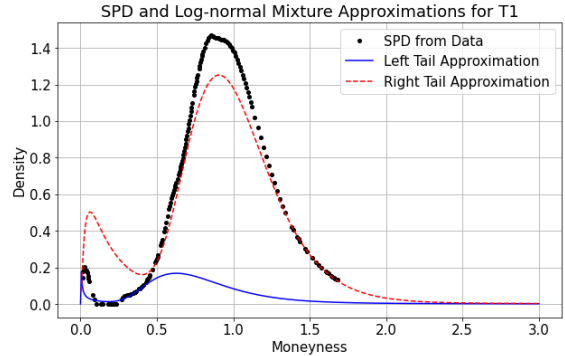Figure 16: Two-lognormal Mixture approximation for Maturity T1

Figure 17: Two-lognormal Mixture approximation for Maturity T1(Showing Whole Tail Estimation by Proposed Method)

At this stage, we have established non-arbitrage state price density functions for all maturities. We utilize spline interpolation to construct the marginal distributions from generated state price densities required for the Bass construction. This process involves deriving both the marginal distributions and their inverses through interpolation or extrapolation from discrete points. Consequently, some interpolation/extrapolation errors are introduced, impacting the accuracy of the final simulation. Unlike the Black-Scholes model, where explicit and smooth mathematical expressions are available for all marginal distributions and their inverses, the presence of interpolation/extrapolation errors offsets the advantages of large-scale Monte Carlo simulations when dealing with market data. Based on our experimental data, we select a simulation size of approximately 7×10^6.

Figures 18 depicts the relationship between calibration accuracy and iteration tolerance across two maturities. Detailed numerical results are provided in table 5 and 6. Since no calibration is required for calculating the IV curve of the first maturity, and by fixing the same set of random seeds, we obtain consistent simulation accuracy for this maturity. Notably, reducing the iteration tolerance from 10^{-3} to 10^{-4} halves the calibration error. However, further reducing the tolerance below 10^{-4} does not lead to significant improvement, as the accuracy level for the first maturity, T_1, is already close to optimal, and error is then dominated by Monte Carlo simulation.

Figure 19 compares the computational time required for different integration schemes. We observe that selecting the Trapezoidal Rule Scheme saves 8 seconds when using an iteration tolerance of 10^{-4} and 20 seconds when using a tolerance of 10^{-5}. These results argues the importance of applying higher accuracy in the calibration process for real market data.
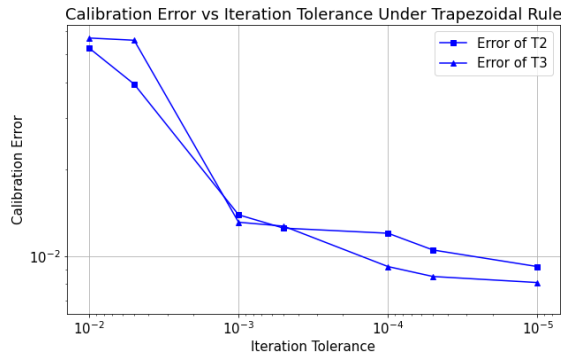

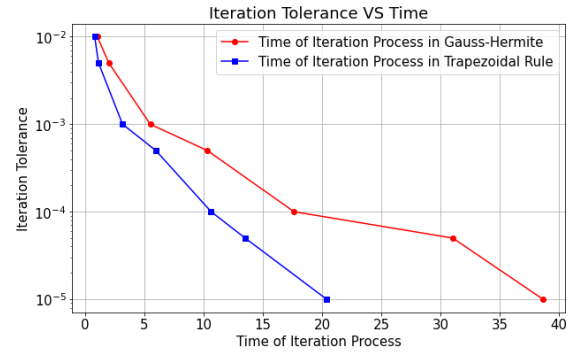Figure 18: Calibration Error VS Iteration Tolerance under Trapezoidal Rule Scheme of Market Case

Figure 19: Time for Iteration Process with Different Tolerance using Two Numerical Schemes for Market Data

Figure 20 demonstrates that the linear convergence rate of the fixed-point algorithm, as established by our proposed method, is consistent even when applied to real market data. Additionally, figure 21 illustrates the IV curve fitting for call options under the iteration tolerance level of 10^{-4}, and this verifies the effectiveness of the proposed model in fitting the market IV curves.

Table 5: Time and Error Outcomes for Gauss Hermite Quadrature under Market Case for Different Maturities

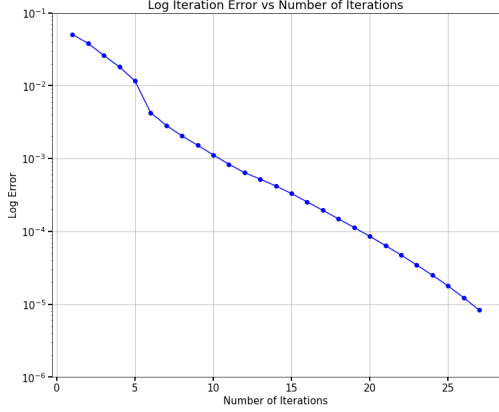| Iteration Tolerance	Iteration Time	Calibration Acc of T_1	Calibration Acc of T_2	Calibration Acc of T_3
1.00E-02	1.033	7.00E-03	4.80E-02	5.68E-02
5.00E-03	2.011	7.00E-03	3.83E-02	5.68E-02
1.00E-03	5.501	7.00E-03	1.73E-02	1.89E-02
5.00E-04	10.321	7.00E-03	1.05E-02	1.17E-02
1.00E-04	17.633	7.00E-03	8.50E-03	8.30E-03
5.00E-05	31.025	7.00E-03	8.30E-03	8.00E-03
1.00E-05	38.635	7.00E-03	8.40E-03	7.80E-03

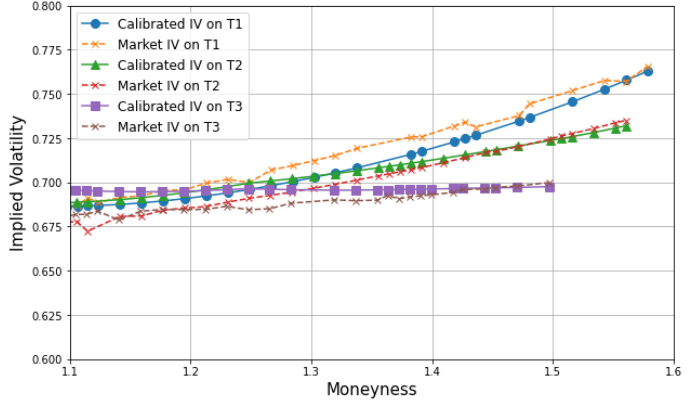Figure 20: Log iteration error vs number of iterations under Market Case

Figure 21: IV Curve Fitting under 1e-4 Iteration Tolerance

Table 6: Time and Error Outcomes for Trapezoidal Rule Scheme under Market Case for Different Maturities

Iteration Tolerance	Iteration Time	Calibration Acc of T_1	Calibration Acc of T_2	Calibration Acc of T_3
1.00E-02	0.812	7.00E-03	5.25E-02	5.69E-02
5.00E-03	1.139	7.00E-03	3.94E-02	5.59E-02
1.00E-03	3.163	7.00E-03	1.39E-02	1.31E-02
5.00E-04	5.975	7.00E-03	1.25E-02	1.27E-02
1.00E-04	10.638	7.00E-03	1.20E-02	9.20E-03
5.00E-05	13.506	7.00E-03	1.05E-02	8.50E-03
1.00E-05	20.378	7.00E-03	9.20E-03	8.10E-03

6 Conclusions

This paper presents a new method for robust and fast calibration of Bass local volatility models. One key step is to accurately construct state price densities from option prices data. Arbitrage free state price densities are obtained using a local quadratic regression approach. Lognormal mixtures are used to model the tails. This approach provides high quality state price densities that ensure accurate Bass LV calibration. After state price densities and the corresponding marginal distributions are obtained, one needs to solve the corresponding fixed point problems to complete Bass LV construction. This involves various convolutions that must be integrated numerically. The simplest trapezoidal rule based schemes turn out to be surprisingly fast and accurate. We study the mathematical optimality and convergence of the trapezoidal schemes, and compare them to commonly used Gauss-Hermite quadrature. Numerical experiments in standard options pricing models as well as in market case studies show that the proposed method for constructing state price densities leads to great calibration robustness and accuracy, and trapezoidal rule based numerical convolution outperforms Gauss-Hermite quadrature for faster calibration of Bass local volatility models.

7 Appendix

7.1 Proofs

7.1.1 Proof of corollary 1

By Theorem 2.4 from [Conze and Henry-Labordere, 2021], we know that the fixed-point algorithm converges under the assumption that $K_\Delta \star F \approx F + \frac{1}{2}\Delta F''$, where $\Delta := T_2 - T_1$. Let $G_i(y) := F_{\mu_i}^{-1}(y)$ for $i = 1, 2$. The inverse solution for F can be expressed as:

$$F^{-1}(u) = \int_{\frac{1}{2}}^u \mathrm{d}y \sqrt{\frac{G_2'(y)}{\frac{2}{\Delta}\int_0^y (G_1(z) - G_2(z))\,\mathrm{d}z}} \tag{20}$$

If G_i are analytic functions and $G_i \neq G_j$ for all $i \neq j$, and given that $G_i = 0$ if and only if $y = 0$, the analytic property will be preserved for $F^{-1}(\mu)$. In the specific case where G_1, G_2 are quantile functions for lognormal distributions, and $G_1 \neq G_2$, the form of G_i is:

$$G_i(p) = \exp\left(\mu_i + \sqrt{2\sigma_i^2}\,\mathrm{erf}^{-1}(2p - 1)\right)$$

where μ_i represents the mean and σ_i the standard deviation of the lognormal distribution, and $\mathrm{erf}^{-1}()$ denotes the inverse of the error function. Recall that the erf function is a map from $\mathbb{R}$ to $(-1, 1)$, and it can be defined as:

$$f(x) = \frac{2}{\sqrt{\pi}}\int_0^x \exp\left(-t^2\right)\mathrm{d}t$$

This erf function is an entire function and has no critical points, i.e., $f'(z) \neq 0$ for $z \in \mathbb{C}$. Since erf function has two finite asymptotic values, ± 1, one can derive analytic property of the inverse erf function, thus the analytic property of the quantile function for the lognormal distribution function.

From the general theory of singularities for the inverse of an analytic function, it follows that if a function has logarithmic singularities at certain points, then its inverse will exhibit these singularities as well. Specifically, if the function has logarithmic singularities at ± 1, then in any simply connected domain that does not contain ± 1, the inverse analytic branches exist.

In particular, there is an inverse branch in the unit disk satisfying $f^{-1}(0) = 0$, and this branch is unique. By applying the Bürmann-Lagrange formula, the inverse erf function can be expressed as a Maclaurin series as follows:

$$\mathrm{erf}^{-1}(z) = \sum_{k=0}^\infty \frac{c_k}{2k+1}\left(\frac{\sqrt{\pi}}{2}z\right)^{2k+1}$$

where $c_0 = 1$ and

$$c_k = \sum_{m=0}^{k-1} \frac{c_m c_{k-1-m}}{(m+1)(2m+1)}$$

Before proceeding, let's recall that the Hardy space H^p is defined as the set of all functions that are analytic in the open unit disk and whose p-th power mean is bounded on each smaller disk. More formally, $f \in H^p$ if

$$\sup_{0<r<1}\left(\frac{1}{2\pi}\int_0^{2\pi}\left|f\left(re^{i\theta}\right)\right|^p\mathrm{d}\theta\right)^{\frac{1}{p}} < \infty$$

Importantly, when $p = 2$, the Hardy space H^2 is a Hilbert space, and the coefficients of the power series of a function in H^2 belong to ℓ^2 by Parseval's theorem.

For our case, this inverse branch has two logarithmic singularities at $(-1, 1)$ is analytic at rest points. It follows that the inverse branch belongs to all H^p for any $p > 0$, in particular, it belongs to H^2, and thus its coefficients belong to ℓ^2 by Parseval.

One thus can combine the Maclaurin series expression and conclude that the inverse error function is analytic over the open unit disk $|z| < 1$, and it has logarithmic singularities at points $z = \pm 1$. Given the solution for $F^{-1}(u)$, one have $y \in \left[\frac{1}{2}, 1\right)$ for $G_1(y), G_2(y), G_2'(y)$. Therefore, $F^{-1}(u)$ is analytic in its defined region. Since the CDF

is non-decreasing, and the analytic inverse function is also monotonic, one can state that $F_{W_{T_i}}^{(n)}$ is analytic under our analytic input assumptions.

Furthermore, in the case of finite smoothness, where G_i are approximated by functions with smoothness order m, the inverse operation similarly preserves the minimum smoothness order across marginal distributions. This guarantees that the fixed-point algorithm's final result, F, inherits the smoothness of the original inputs, completing the proof.

7.1.2 Proof of corollary 2

Recall that for $m \in \mathbb{N}$, the weighted Sobolev space $\mathscr{H}_m$ with the weight function $\rho(x) = \frac{1}{\sqrt{2\pi\sigma^2}}e^{-\frac{x^2}{2\sigma^2}}$ consists of functions $f \in L_\rho^2$ whose weak derivatives up to order m belong to L_ρ^2:

$$\mathscr{H}_m := \left\{ f \in L_\rho^2 \mid \|f\|_m := \left(\sum_{\tau=0}^m \|f^{(\tau)}\|_{L_\rho^2}^2 \right)^{1/2} < \infty \right\},$$

where $L_\rho^2 = \left\{ f : \mathbb{R} \to \mathbb{R} \mid \|f\|_{L_\rho^2}^2 = \int_{\mathbb{R}} |f(x)|^2 \rho(x)\, \mathrm{d}x < \infty \right\}$.

The convolution expression for the inner integrand, $\int_{\mathbb{R}} \rho(y) * F_{\mu_{i+1}}^{-1} \left(\int_{\mathbb{R}} F_{W_{T_i}}(w - y - x)\rho(x)\, \mathrm{d}x \right) \mathrm{d}y$, involves $F_{W_{T_i}}$, a function with smoothness order m. To show that $f = F_{W_{T_i}} \in \mathscr{H}_m$, we need to prove that $\|f\|_m < \infty$ for Bass-LV construction.

For $\tau = 0$, we compute:

$$\left\| f^{(0)} \right\|_{L_\rho^2}^2 = \int_{\mathbb{R}} |f(x)|^2 \rho(x)\, \mathrm{d}x < \int_{\mathbb{R}} \rho(x)\, \mathrm{d}x = 1,$$

since $f(x)$ is a cumulative distribution function, bounded by 1. This shows that $f \in L_\rho^2$.

For $\tau = 1$, with $p_f = f'$, we have:

$$\left\| f^{(1)} \right\|_{L_\rho^2}^2 = \int_{\mathbb{R}} |p_f(x)|^2 \rho(x)\, \mathrm{d}x \leq \max(p_f)^2 \int_{\mathbb{R}} \rho(x)\, \mathrm{d}x = \max(p_f)^2.$$

Here, $\max(p_f)$ is finite due to the smoothness and non-negativity of p_f.

For $\tau > 1$, the function $f^{(\tau)}$ can be expressed as a piecewise smooth function over segments. Denote these segments by $S_j = [a_j, b_j]$, for $j = 1, \ldots, k$, where each segment corresponds to an interval where the function is a polynomial of order $m - \tau$. For the middle segments, where $j = 2, \ldots, k - 1$, we have:

$$\int_{S_j} |f^{(\tau)}(x)|^2 \rho(x)\, \mathrm{d}x \leq \max_j |f^{(\tau)}(x)|^2 \int_{S_j} \rho(x)\, \mathrm{d}x \leq \max_j |f^{(\tau)}(x)|^2.$$

For the boundary segments, $S_1 = (-\infty, a_1]$ and $S_k = [b_k, \infty)$, we evaluate the integral as follows:

$$\int_{b_k}^\infty x^t e^{-x^2/2}\, \mathrm{d}x = 2^{\left(\frac{t-1}{2} \right)} \left(\int_{\frac{b_k^2}{2}}^\infty e^{-y} y^{\frac{t-1}{2}}\, \mathrm{d}y - \left[y^{\frac{t-1}{2}} e^{-y} \right]_{b_k}^\infty \right).$$

It is clear that the term $\left[y^{\frac{t-1}{2}} e^{-y} \right]_{b_k}^\infty = 0$ for any t, and the integral $\int_{\frac{b_k^2}{2}}^\infty e^{-y} y^{\frac{t-1}{2}}\, \mathrm{d}y$ is finite for $t \geq 0$.

Now, if $\frac{t-1}{2}$ is an integer, the integration will eventually reduce to $\int_{\frac{b_k^2}{2}}^\infty e^{-y}\, \mathrm{d}y + C$, where C is a finite constant. If $\frac{t-1}{2}$ is not an integer, after a finite number of iterations, we arrive at an integral of the form $\int_{\frac{b_k^2}{2}}^\infty e^{-y} y^{\frac{t-q}{2}}\, \mathrm{d}y$, where $\frac{t-q}{2} < 0$, which is clearly finite since the exponential decay dominates for large y.

By similar reasoning, for the segment $S_1 = (-\infty, a_1]$, we apply the same steps and conclude that the integral over this region is also finite. In this case, the polynomial term grows negatively, but the exponential decay of $\rho(x)$ as $x \to -\infty$ ensures that the integral converges in Bass-LV construction.

Thus, both boundary integrals converge, and since there are only $k - 2$ middle segments with finite upper bounds, we conclude that $\left\| f^{(\tau)} \right\|_{L_\rho^2}^2$ is finite for all $\tau \in (1, m]$. As m is a finite smoothness order, the sum $\sum_{\tau=0}^m \left\| f^{(\tau)} \right\|_{L_\rho^2}^2$ is bounded from above, and therefore finite.

Consequently, the inner integrand is well-defined in the weighted Sobolev space. For the outer integrand, $F_{\mu_{i+1}}^{-1}$, which is a piecewise polynomial, similar analysis applies, showing that it is also well-defined in $\mathscr{H}_m$.

Finally, by applying results from [Kazashi et al., 2023] and [Mastroianni and Monegato, 1994], we derive the convergence rate for Gauss-Hermite quadrature in the weighted Sobolev space $\mathscr{H}_m$. Specifically, for a function $f \in \mathscr{H}_m$, the Gauss-Hermite quadrature approximation $Q_n^{\mathrm{GH}}(f)$ to the integral $I(f) := \int_{\mathbb{R}} f(x)\rho(x)\,\mathrm{d}x$, where $\rho(x)$ is the Gaussian weight function, satisfies the following error bound:

$$\left|I(f) - Q_n^{\mathrm{GH}}(f)\right| \le Cn^{-m/2}\|f\|_m,$$

where n is the number of quadrature points, m is the smoothness order of the function f, $\|f\|_m$ is the norm in the weighted Sobolev space, and $C > 0$ is a constant independent of n.

This result shows that the convergence rate of the Gauss-Hermite quadrature depends on both the number of quadrature points n and the smoothness m of the function f. As n increases, the error decays at a rate proportional to $n^{-m/2}$, with smoother functions (i.e., higher m) leading to faster convergence. The constant C is determined by the specific properties of the function and the quadrature scheme but remains independent of the number of quadrature points.

To be brief, we conclude that in Bass-LV construction, the rate of convergence for Gauss-Hermite quadrature under finite smoothness condition can achieve $\mathcal{O}\left(n^{-m/2}\right)$. Now we complete the proof for this part.

7.1.3 Proof of Proposition 1

Before deriving the optimality of the Trapezoidal Rule Scheme, we first present some properties of Hermite polynomials, which will be useful for our weighted function $\rho(x) = \frac{1}{\sqrt{2\pi\sigma^2}}e^{-\frac{x^2}{2\sigma^2}}$. Recall that the probabilist's Hermite polynomials are defined as:

$$He_n(x) = (-1)^n e^{\frac{x^2}{2}} \frac{d^n}{dx^n} e^{-\frac{x^2}{2}},$$

and satisfy the orthogonality relation:

$$\int_{-\infty}^{\infty} He_m(x)He_n(x)e^{-\frac{x^2}{2}}\,dx = \sqrt{2\pi}n!\delta_{nm},$$

where δ_{nm} is the Kronecker delta. We now state the following corollary:

Corollary 3. *The normalized Hermite polynomials with respect to $\rho(x)$ are given by:*

$$H_{e_n}^{\sigma}(x) = \frac{(-1)^n\sigma^n}{\sqrt{n!}}e^{\frac{x^2}{2\sigma^2}}\frac{d^n}{dx^n}e^{-\frac{x^2}{2\sigma^2}}, \quad x \in \mathbb{R},$$

and satisfy the recurrence relation:

$$(H_{e_n}^{\sigma}(x))' = \sqrt{n}H_{e_{n-1}}^{\sigma}(x), \quad \forall n \ge 1.$$

Proof: First, we verify the normalization by calculating the L_ρ^2 norm:

$$\int_{-\infty}^{\infty} H_{e_n}^{\sigma}(x)H_{e_n}^{\sigma}(x)\rho(x)dx = 1.$$

This follows directly from applying the orthogonality relation of the Hermite polynomials, and adjusting for the scaling factor σ:

$$\int_{-\infty}^{\infty} H_{e_n}^{\sigma}(x)H_{e_n}^{\sigma}(x)\frac{1}{\sqrt{2\pi\sigma^2}}e^{-\frac{x^2}{2\sigma^2}}\,dx$$

$$= \frac{\sigma^{2n}}{n!\sqrt{2\pi}}\int_{-\infty}^{\infty}\left[e^{\frac{x^2}{2\sigma^2}}\frac{d^n}{dx^n}e^{-\frac{x^2}{2\sigma^2}}\right]^2 e^{-\frac{x^2}{2\sigma^2}}\frac{1}{\sigma}dx$$

$$= \frac{\sigma^{2n}}{n!\sqrt{2\pi}}\int_{-\infty}^{\infty}\left[e^{\frac{y^2}{2}}\frac{1}{\sigma^n}\frac{d^n}{dy^n}e^{-\frac{y^2}{2}}\right]^2 e^{-\frac{y^2}{2}}\,dy$$

$$= \frac{1}{n!\sqrt{2\pi}}\int_{-\infty}^{\infty} He_n(y)He_n(y)e^{-\frac{y^2}{2}}\,dy$$

$$= \frac{1}{n!\sqrt{2\pi}}\sqrt{2\pi}n! = 1$$

The recurrence relation is derived using the chain rule on the differentiated form of $H_{e_n}^\sigma(x)$, applying the Leibniz rule for products of exponentials and polynomials:

$$\left(H_{e_n}^\sigma(x)\right)' = \frac{(-1)^n \sigma^n}{\sqrt{n!}} \left(e^{\frac{x^2}{2\sigma^2}} D^n \left(e^{-\frac{x^2}{2\sigma^2}}\right)\right)'$$

$$= \frac{(-1)^n \sigma^n}{\sqrt{n!}} \left[\frac{x}{\sigma} e^{\frac{x^2}{2\sigma^2}} D^n \left(e^{-\frac{x^2}{2\sigma^2}}\right) + e^{\frac{x^2}{2\sigma^2}} D^n \left(-\frac{x}{\sigma} e^{-\frac{x^2}{2\sigma^2}}\right)\right]$$

$$= \frac{(-1)^n \sigma^n}{\sqrt{n!}} \left[\frac{x}{\sigma} e^{\frac{x^2}{2\sigma^2}} D^n \left(e^{-\frac{x^2}{2\sigma^2}}\right) + e^{\frac{x^2}{2\sigma^2}} \sum_{k=1}^n \binom{n}{k} D^k \left(-\frac{x}{\sigma}\right) D^{n-k} \left(e^{-\frac{x^2}{2\sigma^2}}\right)\right]$$

$$= \frac{(-1)^n \sigma^n}{\sqrt{n!}} \left[\frac{x}{\sigma} e^{\frac{x^2}{2\sigma^2}} D^n \left(e^{-\frac{x^2}{2\sigma^2}}\right) + e^{\frac{x^2}{2\sigma^2}} \left(\left(-\frac{x}{\sigma}\right) D^n \left(e^{-\frac{x^2}{2\sigma^2}}\right) + n\frac{-1}{\sigma} D^{n-1} \left(e^{-\frac{x^2}{2\sigma^2}}\right)\right)\right]$$

$$= \frac{(-1)^n \sigma^n}{\sqrt{n!}} \left[e^{\frac{x^2}{2\sigma^2}} D^{n-1} \left(e^{-\frac{x^2}{2\sigma^2}}\right)\right] \frac{(-n)}{\sigma}$$

$$= H_{e_{n-1}}^\sigma(x) \frac{(-1)\sigma}{\sqrt{n}} \frac{(-n)}{\sigma} = \sqrt{n} H_{e_{n-1}}^\sigma(x)$$

We will use this result to bound the norms of the function in the next part of the proof.

Lemma 1 (Bounded Norms). Assume the inner integrand of the Bass-LV construction has m-order smoothness. Let $F_i(x) := F_{W_{T_i}}(w - x - y) \cdot \rho(x)$, where w, y are constants, and $\rho(x) = \frac{1}{\sqrt{2\pi\sigma^2}} e^{-\frac{x^2}{2\sigma^2}}$ is the Gaussian weight function. For the τ-th order derivative of $F_i(x)$, we have the following bounds:

$$\|F_i^{(\tau)}(x)\|_{L^1(\mathbb{R})} < \infty, \quad \|F_i^{(m)}(x)\|_{L^2(\mathbb{R})} < \infty, \quad \sup_{x \in \mathbb{R}} \left|e^{(1-\varepsilon)\frac{x^2}{2\sigma^2}} F_i^{(\tau)}(x)\right| < \infty,$$

where ε is a small positive constant such that $\frac{1-\epsilon}{\sigma^2} \in (0,1)$.

Proof: Since our weighted function is heat kernel with zero drift, it aligns with the form of Hermite quadrature we constructed in corollary 3. We can write under chain rule that:

$$\|F_i^{(\tau)}\|_{L^1(\mathbb{R})} \leq \sum_{k=0}^\tau \binom{\tau}{k} \|F_{W_{T_i}}^{(\tau-k)}(w - x - y) \cdot \rho^{(k)}(x)\|_{L^1}$$

$$= \sum_{k=0}^\tau \binom{\tau}{k} \left(\int_{\mathbb{R}} |F_{W_{T_i}}^{(\tau-k)}(w - x - y) \frac{(-1)^k}{\sigma^k} \sqrt{k!} H_{e_k}^\sigma(x) \frac{1}{\sqrt{2\pi\sigma^2}} e^{-\frac{x^2}{2\sigma^2}}| \, \mathrm{d}x\right)$$

(Applying Hölder's Inequality)

$$\leq \sum_{k=0}^\tau \binom{\tau}{k} \frac{\sqrt{k!}}{\sigma^k} \left(\int_{\mathbb{R}} |F_{W_{T_i}}^{(\tau-k)}(w - x - y)|^2 \rho(x) \, \mathrm{d}x\right)^{1/2} \left(\int_{\mathbb{R}} |H_{e_k}^\sigma(x)|^2 \rho(x) \, \mathrm{d}x\right)^{1/2}.$$

Given that $F_{W_{T_i}}(w - x - y)$ is a m order polynominal in every segments shown in corollary 2, by similar analysis, we can conclude that $\left(\int_{\mathbb{R}} \left|F_{W_{T_i}}^{(\tau-k)}(w - x - y)\right|^2 \rho(x) \, \mathrm{d}x\right)$ is bounded by some constants:

$$\left(\int_{\mathbb{R}} \left|F_{W_{T_i}}^{(\tau-k)}(w - x - y)\right|^2 \rho(x) \, \mathrm{d}x\right) < C_{F_w}^{(\tau-k)},$$

where $C_{F_w}^{(\tau-k)}$ is some posivie constant.

By corollary 3, we know that $\left(\int_{\mathbb{R}} \left|H_{e_k}^\sigma(x)\right|^2 \rho(x) \mathrm{d}x\right) = 1 < \infty$. With these analyses, we can then obtain the following:

$$\left\|F_i^{(\tau)}\right\|_{L^1(\mathbb{R})} \leq \sum_{k=0}^\tau \binom{\tau}{k} \frac{\sqrt{k!}}{\sigma^k} (C_{F_w}^{(\tau-k)})^{\frac{1}{2}} < \infty \tag{21}$$

Now we complete the first part of the proof.

For the L^2 norm, since $\int_{\mathbb{R}} \left| H_{e_k}^{\sigma}(x) \right|^2 \rho(x) \mathrm{d}x = 1$, there must exist a supremum C_H such that $\left| H_{e_k}^{\sigma}(x) \right|^2 \rho(x) < C_H, \forall x \in \mathbb{R}$. Therefore, we can write the following:

$$
\begin{aligned}
\left\| F_i^{(m)} \right\|_{L^2(\mathbb{R})} &\leq \sum_{k=0}^{m} \binom{m}{k} \left(\int_{\mathbb{R}} \left| F_{W_{T_i}}^{(m-k)}(w - y - x) \frac{(-1)^k}{\sigma^k} \sqrt{k!} H_{e_k}^{\sigma}(x) \frac{1}{\sqrt{2\pi\sigma^2}} e^{-\frac{x^2}{2\sigma^2}} \right|^2 \mathrm{d}x \right)^{\frac{1}{2}} \\
&\leq \sum_{k=0}^{m} \binom{m}{k} \left(C_H \frac{k!}{\sigma^{2k}} \int_{\mathbb{R}} \left| F_{W_{T_i}}^{(m-k)}(w - y - x) \right|^2 \rho(x) dx \right)^{\frac{1}{2}} \\
&< \sum_{k=0}^{m} \binom{m}{k} \left(C_H \frac{k!}{\sigma^{2k}} C_{F_w}^{(m-k)} \right)^{\frac{1}{2}} < \infty
\end{aligned}
$$

For the infinity norm, we denote $e^{\frac{(1-\epsilon)x^2}{2\sigma^2}} = \rho(x)^{\epsilon-1}$. Note that $H_{e_k}^{\sigma}(x)$ is a k-th order polynomial, i.e., the asymptotic behavior of $H_{e_k}^{\sigma}(x)$ is $O(x^k)$. We first establish that there exists a finite supremum $C_H^{\epsilon_1}$ for the product $F_H(x) := H_{e_k}^{\sigma}(x)\rho^{\epsilon_1}(x)$, where $\epsilon_1 > 0$ and $x \in \mathbb{R}$.

Since $\rho(x) = \frac{1}{\sqrt{2\pi\sigma^2}} e^{-\frac{x^2}{2\sigma^2}}$, for any $\epsilon_1 > 0$, $\rho(x)$ decays exponentially as $x \to \pm\infty$, while $H_{e_k}^{\sigma}(x)$, as a polynomial, can increase or decrease at most polynomially in x. Therefore, the product $F_H(x)$ exhibits a finite bound as $x \to \pm\infty$.

Furthermore, for any sufficiently large but finite interval $[a, b]$, $F_H(x)$ is continuous by construction. By applying the extreme value theorem, we conclude that it attains finite upper and lower bounds on any such interval. Now consider $G_W(x) := F_{W_{T_i}}^{(\tau)}(w - y - x)\rho^{\epsilon_2}(x)$, where $\epsilon_2 > 0$ and w, y are constants. Similar to the previous case, we examine the behavior of $G_W(x)$ as $x \to \pm\infty$.

From the analysis in Corollary 2, we know that $F_{W_{T_i}}^{(\tau)}$ is a piecewise polynomial function on the interval $(-\infty, s_1], [s_k, \infty)$, and hence it is bounded as $x \to \pm\infty$. By applying the extreme value theorem again, we establish that $G_W(x)$ has a finite supremum, denoted $C_{F_w^{(\tau)}}^{\epsilon_2}$, for any given $\epsilon_2 > 0$ and derivative order τ.

Thus, we conclude that for the supremum norm:

$$
\sup_{\substack{x \in \mathbb{R} \\ \tau \in \{0, \ldots, m-1\}}} \left| e^{(1-\varepsilon)\frac{x^2}{2\sigma^2}} F_i^{(\tau)}(x) \right|
$$

we have:

$$
\begin{aligned}
&\left\| e^{(1-\varepsilon)\frac{x^2}{2\sigma^2}} F_i^{(\tau)}(x) \right\|_{L^{\infty}(\mathbb{R})} \\
&\leq \sum_{k=0}^{\tau} \binom{\tau}{k} \left\| \rho(x)^{\epsilon-1} F_{W_{T_i}}^{(\tau-k)}(w - y - x)\rho^{(k)}(x) \right\|_{L^{\infty}(\mathbb{R})} \\
&= \sum_{k=0}^{\tau} \binom{\tau}{k} \left\| \rho(x)^{\epsilon-1} F_{W_{T_i}}^{(\tau-k)}(w - y - x)\rho(x) H_{e_k}^{\sigma}(x) \frac{(-1)^k \sqrt{k!}}{\sigma^k} \right\|_{L^{\infty}(\mathbb{R})} \\
&\leq \sum_{k=0}^{\tau} \binom{\tau}{k} \left\| \rho(x)^{\frac{\epsilon}{2}} F_{W_{T_i}}^{(\tau-k)}(w - y - x) \right\|_{L^{\infty}(\mathbb{R})} \left\| H_{e_k}^{\sigma}(x) \frac{(-1)^k \sqrt{k!}}{\sigma^k} \rho(x)^{\frac{\epsilon}{2}} \right\|_{L^{\infty}(\mathbb{R})} \\
&\leq \sum_{k=0}^{\tau} \binom{\tau}{k} C_H^{\frac{\epsilon}{2}} \frac{\sqrt{k!}}{\sigma^k} C_{F_w^{(\tau-k)}}^{\frac{\epsilon}{2}}
\end{aligned}
$$

By construction, we need choose $\epsilon \in (max\{0, 1 - \sigma^2\}, 1)$. In the last inequality, we obtain the supermum by setting $\epsilon_1 = \epsilon_2 = \frac{\epsilon}{2}$. Since $\tau \in [0, m-1]$ is finite, the finite summation of bounded values is finite, thus giving $\sup_{\substack{x \in \mathbb{R} \\ \tau \in \{0, \ldots, m-1\}}} \left| e^{(1-\varepsilon)\frac{x^2}{2\sigma^2}} F_i^{(\tau)}(x) \right| < \infty$.

Application of Theorem: With the above lemma established, we now apply the results from [Kazashi et al., 2023], Proposition 4.2, to our numerical setup in the Bass-LV model.

Theorem (Kazashi 2023, Proposition 4.2): Let $m \in \mathbb{N}$ represent the smoothness order of the function g. Assume that $g^{(\tau)} : \mathbb{R} \to \mathbb{R}$ is absolutely continuous on any compact interval for each derivative order $\tau = 0, \ldots, m-1$, and that the m-th derivative, $g^{(m)}$, belongs to the space $L^2(\mathbb{R})$ (the space of square-integrable functions). Additionally, g must satisfy the following two conditions:

1. Local Regularity: The m-th order Sobolev norm of g, denoted as $\|g\|_m^*$, is uniformly bounded over all compact intervals $I \subset \mathbb{R}$. This norm is defined as:

$$\|g\|_m^* := \sup_{\substack{I \subset \mathbb{R} \\ |I| < \infty}} \|g\|_{m,I} := \sup_{\substack{I \subset \mathbb{R} \\ |I| < \infty}} \left(\sum_{\tau=0}^{m-1} \left(\int_I g^{(\tau)}(x)\, dx \right)^2 + \int_I \left| g^{(m)}(x) \right|^2 dx \right)^{1/2}.$$

This norm ensures that g and its derivatives up to order m are well-behaved over compact intervals.

2. Decay at Infinity: The function g must exhibit a controlled decay at infinity, expressed as:

$$\|g\|_{m,\text{decay}} := \sup_{\substack{x \in \mathbb{R} \\ \tau \in \{0,\ldots,m-1\}}} \left| e^{(1-\varepsilon)\frac{x^2}{2}} g^{(\tau)}(x) \right| < \infty, \quad \text{for some } \varepsilon \in (0,1).$$

This condition ensures that $g(x)$ and its derivatives decay rapidly enough as $x \to \pm\infty$, governed by the exponential decay factor $e^{(1-\varepsilon)\frac{x^2}{2}}$.

Given these assumptions, the error for the n-point Trapezoidal Rule Scheme $Q_{n,T}^*(g)$ with a cutoff interval $[-T, T]$ is bounded by:

$$\left| \int_{\mathbb{R}} g(x)\, dx - Q_{n,T}^*(g) \right| \leq C \left(\|g\|_m^* + \|g\|_{m,\text{decay}} \right) \frac{(\ln n)^{m/2+1/4}}{n^m},$$

where C is a constant independent of n and g, but dependent on m and ε. Here, the Trapezoidal Rule approximation $Q_{n,T}^*(g)$ is given by:

$$Q_{n,T}^*(g) := \frac{2T}{n} \sum_{j=0}^{n-1} g\left(\xi_j^* \right),$$

where $\xi_j^* := \frac{2T}{n} j - T$, and $T = \sqrt{\frac{2}{(1-\varepsilon)} m \ln n}$ is the cutoff interval.

Adaptation for Bass-LV Model: In the Bass-LV implementation, we modify the theorem to match the specifics of our integrand $g(x)$, which is given by:

$$g(x) = F_{W_{T_i}}(w - y - x) \cdot \rho(x),$$

where $\rho(x) = \frac{1}{\sqrt{2\pi\sigma^2}} e^{-\frac{x^2}{2\sigma^2}}$ is the weighted function representing the heat kernel. The prerequisite for $g(x)$ is satisfied in our proof above, the parameters w and y are constants, and $F_{W_{T_i}}(w - y - x)$ is the piecewise polynomial representation of the unknown distribution function at maturity T_i.

We set $T = Mh$, $n = 2M + 1 \geq 2$, and $h = \frac{2T}{n}$, where M is the number of quadrature points used. The term $1 - \varepsilon$ is adjusted to reflect the variance in the heat kernel, given by:

$$1 - \varepsilon = \frac{1 - \epsilon}{\sigma^2}, \quad \epsilon \in (max\{1 - \sigma^2, 0\}, 1),$$

where $\sigma^2 = T_{i+1} - T_i$ represents the time interval between maturities T_i and T_{i+1}.

Applying these modifications, we derive the optimal parameter settings for the Trapezoidal Rule Scheme for the inner integrand as follows:

$$Mh = \sqrt{\frac{2(T_{i+1} - T_i)}{(1 - \epsilon)} m \ln(2M + 1)}, \quad h = \frac{\sqrt{\frac{2(T_{i+1} - T_i)}{(1 - \epsilon)} m \ln(2M + 1)}}{M}.$$

Outer Integrand: The outer integrand, $F_{\mu_{i+1}}^{-1}$, is represented by a finite-order smoothness spline interpolation. Since the inputs to this function are also finite, similar results for optimality can be applied to the outer integrand, by imposing its own smoothness order and choosing ϵ independently within the interval $\epsilon \in (\max\{1 - \sigma^2, 0\}, 1)$.

Convergence Rate: From the results above, we conclude that the convergence rate of the Trapezoidal Rule Scheme for a single integrand in the Bass-LV implementation is:

$$\mathcal{O}\left(\frac{(\ln n)^{m/2+1/4}}{n^m}\right),$$

where m is the smoothness order of the integrand, and n represents the number of points counted in the Trapezoidal Rule.

Disclaimer

This paper was prepared for informational purposes in part by the Quantitative Research Group of JPMorgan Chase & Co. This paper is not a product of the Research Department of JPMorgan Chase & Co. or its affiliates. Neither JPMorgan Chase & Co. nor any of its affiliates makes any explicit or implied representation or warranty and none of them accept any liability in connection with this paper, including, without limitation, with respect to the completeness, accuracy, or reliability of the information contained herein and the potential legal, compliance, tax, or accounting effects thereof. This document is not intended as investment research or investment advice, or as a recommendation, offer, or solicitation for the purchase or sale of any security, financial instrument, financial product or service, or to be used in any way for evaluating the merits of participating in any transaction.

References

Antoine Conze and Pierre Henry-Labordere. Bass construction with multi-marginals: Lightspeed computation in a new local volatility model. *Available at SSRN 3853085*, 2021.

Emanuel Derman, Iraj Kani, and Joseph Z Zou. The local volatility surface: Unlocking the information in index option prices. *Financial analysts journal*, 52(4):25–36, 1996.

Thomas F Coleman, Yuying Li, and Arun Verma. Reconstructing the unknown local volatility function. In *Quantitative Analysis In Financial Markets: Collected Papers of the New York University Mathematical Finance Seminar (Volume II)*, pages 192–215. World Scientific, 2001.

Mohamed Bouzoubaa and Adel Osseiran. *Exotic options and hybrids: A guide to structuring, pricing and trading*. John Wiley & Sons, 2010.

Antonie Kotzé, Rudolf Oosthuizen, and Edson Pindza. Implied and local volatility surfaces for south african index and foreign exchange options. *Journal of Risk and Financial Management*, 8(1):43–82, 2015.

Julio Backhoff, Mathias Beiglböck, Martin Huesmann, and Sigrid Källblad. Martingale benamou–brenier: a probabilistic perspective. *arXiv preprint arXiv:1708.04869*, 2017.

Beatrice Acciaio, Antonio Marini, and Gudmund Pammer. Calibration of the bass local volatility model. *arXiv preprint arXiv:2311.14567*, 2023.

Bertram Tschiderer. q-bass martingales. *arXiv preprint arXiv:2402.05669*, 2024.

Gregoire Loeper. The measure preserving martingale sinkhorn algorithm. *arXiv preprint arXiv:2310.13797*, 2023.

Julio Backhoff-Veraguas, Walter Schachermayer, and Bertram Tschiderer. The bass functional of martingale transport. *arXiv preprint arXiv:2309.11181*, 2023a.

Julio Backhoff-Veraguas, Mathias Beiglböck, Walter Schachermayer, and Bertram Tschiderer. The structure of martingale benamou brenier in r^d. *arXiv preprint arXiv:2306.11019*, 2023b.

Gaspard Monge. Mémoire sur la théorie des déblais et des remblais. *Mem. Math. Phys. Acad. Royale Sci.*, pages 666–704, 1781.

Pierre Henry-Labordere. From (martingale) schrodinger bridges to a new class of stochastic volatility model. *Available at SSRN 3353270*, 2019a.

Hadrien De March and Pierre Henry-Labordere. Building arbitrage-free implied volatility: Sinkhorn's algorithm and variants. *arXiv preprint arXiv:1902.04456*, 2019.

Stephan Eckstein and Michael Kupper. Computation of optimal transport and related hedging problems via penalization and neural networks. *Applied Mathematics & Optimization*, 83(2):639–667, 2021.

Pierre Henry-Labordere. (martingale) optimal transport and anomaly detection with neural networks: A primal-dual algorithm. *arXiv preprint arXiv:1904.04546*, 2019b.

David Hobson and Anthony Neuberger. Robust bounds for forward start options. *Mathematical Finance: An International Journal of Mathematics, Statistics and Financial Economics*, 22(1):31–56, 2012.

Mathias Beiglböck, Pierre Henry-Labordere, and Friedrich Penkner. Model-independent bounds for option prices—a mass transport approach. *Finance and Stochastics*, 17:477–501, 2013.

Yan Dolinsky and H Mete Soner. Martingale optimal transport and robust hedging in continuous time. *Probability Theory and Related Fields*, 160(1):391–427, 2014.

Pierre Henry-Labordère and Nizar Touzi. An explicit martingale version of the one-dimensional brenier theorem. *Finance and Stochastics*, 20:635–668, 2016.

Ivan Guo, Grégoire Loeper, and Shiyi Wang. Local volatility calibration by optimal transport. *arXiv preprint arXiv:1709.08075*, 2017.

Pierre Henry-Labordère. *Model-free hedging: A martingale optimal transport viewpoint*. Chapman and Hall/CRC, 2017.

Marcel Nutz, Johannes Wiesel, and Long Zhao. Martingale schrödinger bridges and optimal semistatic portfolios. *Finance and Stochastics*, 27(1):233–254, 2023.

Michal Benko, Matthias Fengler, Wolfgang Härdle, and Milos Kopa. On extracting information implied in options. *Computational statistics*, 22:543–553, 2007.

Bernhard Brunner and Reinhold Hafner. Arbitrage-free estimation of the risk-neutral density from the implied volatility smile. *Journal of Computational Finance*, 7(1):75–106, 2003.

Matthias R Fengler and Lin-Yee Hin. A simple and general approach to fitting the discount curve under no-arbitrage constraints. *Finance research letters*, 15:78–84, 2015.

Yoshihito Kazashi, Yuya Suzuki, and Takashi Goda. Suboptimality of gauss–hermite quadrature and optimality of the trapezoidal rule for functions with finite smoothness. *SIAM Journal on Numerical Analysis*, 61(3):1426–1448, 2023.

Jim Gatheral and Antoine Jacquier. Arbitrage-free svi volatility surfaces. *Quantitative Finance*, 14(1):59–71, 2014.

Justin Birru and Stephen Figlewski. The impact of the federal reserve's interest rate target announcement on stock prices: A closer look at how the market impounds new information. *Script. New York University Stren School of Business*, 2010.

Lykourgos Alexiou, Amit Goyal, Alexandros Kostakis, and Leonidas Rompolis. Pricing event risk: Evidence from concave implied volatility curves. *Swiss Finance Institute Research Paper*, (21-48), 2023.

G Mastroianni and Giovanni Monegato. Error estimates for gauss-laguerre and gauss-hermite quadrature formulas. In *Approximation and Computation: A Festschrift in Honor of Walter Gautschi: Proceedings of the Purdue Conference, December 2–5, 1993*, pages 421–434. Springer, 1994.